Hybrid Model for Smoke and Heat Propagation in Complex Structures

by

Xiaobo Zhu

A thesis submitted to

the Faculty of Graduate Studies and Research

in partial fulfillment of the requirements for the degree of

Master of Science

School of Mathematics and Statistics

Ottawa-Carleton Institute for Mathematics and Statistics

Carleton University

Ottawa, Ontario, Canada

August, 2009

Your file Votre référence
ISBN: 978-0-494-60211-9
Our file Notre référence
ISBN: 978-0-494-60211-9

Abstract

Predicting smoke movement caused by fires is a very important research area of fire and smoke safety. In this thesis, we developed a hybrid of zone and network fire model which simulates smoke and heat movement within fires in multi-compartment buildings. A two-zone model is used to simulate fire and smoke movement inside the room where fire originates and compartments surrounding the fire room. A network model, which predicts both mass and energy flow, is used to simulate smoke movement for the remaining compartments that are far away from the fire room. Appropriate conditions are devised at the interface between the two models.

An approach of decoupling pressure and temperature equations within the network model is used due to their significantly different convergence speeds. A Newton-GMRES method is chosen for finding the solution for the pressures, and a DLSODE ODE solver is used to solve the temperatures.

Various examples with different room configurations are performed and demonstrated in this work, to show that the model is capable of predicting smoke movement in multi-compartment buildings.

Acknowledgments

I would like to thank my supervisors, Dr. David Amundsen and Dr. George Hadjisophocleous for their time, guidance, and effort spent on my thesis.

I would like to thank Dr. Ahmed Kashef, at NRC, for giving me advice and help on my research.

I would like to thank Montu Das, who has been working with me closely in the initial stages of this project, for kindly giving me support especially on the background of fire safety and the development of the model.

I would like to thank my wife Ling for her endless love, encouragement and understanding.

I would like to thank my parents and my sister for their limitless support to improve myself.

Last but not least, I would like to thank all my friends for their support and care.

Contents

List of Figures

List of Tables

List of Symbols

- Ae_i: Effective orifice area on the i^{th} floor.
- A_{Rij}: Area of the opening.
- A_S: Cross-sectional area of the stair shaft.
- A_v: Vent area.
- $A_{Wi(k)}$: Area of the k^{th} wall surface of compartment i.
- B: Width of the opening.
- C_{CV}: Coefficient of ceiling vent flow.
- C_D: Flow coefficient.
- C_{E1},C_{E2}: Constant coefficients.
- C_{LOL}: Limiting coefficient.
- C_p: Specific heat capacity at constant pressure.
- C_{pi}: Specific heat capacity of air for compartment i.
- C_v: Specific heat capacity at constant volume.
- CRP: Carbon related products.
- D_e: Equivalent diameter.
- d_i: Density of people on the stairs between i^{th} floor and $(i-1)^{th}$ floor.

- $\triangle E_{Ai}$: Rate of heat absorbed by the indoor gases per unit time.
- $\dot{E}_{hi}$: Rate of the net heat gain of layer i by heat transfer or combustion.
- E_i: Internal energy in layer/compartment i.
- E_{Li}: Rate of heat carried out by the fire plume through the opening per unit time.
- E_{Ri}: Rate of radiative heat loss through the opening per unit time.
- E_{Wi}: Rate of heat absorbed by the wall surfaces per unit time.
- FO_P: Actual fuel to oxygen ratio in fire plume.
- FO_S: Stoichiometric fuel to oxygen ratio.
- Gr: Grashof number.
- H: Height of the room.
- $HC1$,HCN: Harmful species.
- h_i: Height of the shaft between i^{th} floor and $(i-1)^{th}$ floor.
- $\dot{h}_i$: Rate of enthalpy added to layer i.
- $h_{i(k)}$: Surface heat exchange coefficient of the k^{th} wall surface of compartment i.
- H_n: Hessenberg matrix with size n.
- $\dot{h}_L$: Rate of enthalpy added to the lower layer.

- $\dot{h}_U$: Rate of enthalpy added to the upper layer.
- $(\triangle H)_F$: Effective heat of combustion per unit kilogram fuel in open air.
- $(\triangle H)_O$: Heat of combustion per unit kilogram oxygen.
- g: Acceleration due to gravity.
- k: Friction pressure loss coefficient.
- m_{BF}: Mass of total burnt fuel.
- $\dot{m}_{BF}$: total burnt fuel rate.
- m_{CHO}: Mass of the fuel pyrolysis excluding m_{PFmin}.
- m_{CO}: Mass production of CO.
- m_{CO_2}: Mass production of CO_2.
- m_{CRP}: Mass production of carbon related products of combustion.
- $\dot{m}_e$: Plume entrainment rate.
- m_{H_2O}: Mass production of H_2O.
- m_i: Mass in layer/compartment i.
- $\dot{m}_{i,j}$: Mass flow rate from node i to node j.
- $\dot{m}_{j,i}$: Mass flow rate from node j to node i.
- $\dot{m}_L$: Net mass gain rate of the lower layer.
- $\dot{m}_{O_2}$: Oxygen consumption rate.

- $\dot{m}_{PF}$: Mass pyrolysis rate.
- m_{O_2}: Mass of oxygen.
- m_{PF}: Mass of fuel pyrolysis.
- m_{PFmin}: Harmful species, component of m_{PF}.
- m_{Soot}: Mass production of soot.
- $M_{sup,i}$: Mass source or sink in node i.
- m_{tox1},m_{tox2},m_{tox3}: Toxic species, components of m_{PFmin}.
- m_{TUF}: Mass production of total unburned fuel.
- $\dot{m}_U$: Net mass gain rate of the upper layer.
- M_W: Molecular weight.
- N_{ss}: Neutral plane height.
- P: pressure.
- $P_i(0)$,$P_j(0)$: Pressure of the compartment of each side of the opening i and j at a reference level.
- $P_i(z)$,$P_j(z)$: Pressure of the compartment of each side of the opening i and j at arbitrary height z.
- P_{ij}:Pressure difference of compartment i and j at an opening.
- $\triangle P$: Pressure difference between two compartments.

- $\triangle P(0)$: Pressure difference between two sides of an opening at reference level.
- $\triangle P(z)$: Pressure difference between two sides of an opening at a height z.
- Q: Actual heat release rate.
- Q_c: Convection heat release rate.
- $\dot{Q}_i$: Energy source or sink source.
- Q_N: Heat release rate in unconstrained combustion.
- R: Universal gas constant.
- T_i: Temperature in layer/compartment i.
- T_I: Interface temperature.
- T_L: Lower layer temperature.
- T_U: Upper layer temperature.
- $T_{Wi(k)}$: Surface temperature of the k^{th} wall surface of compartment i.
- V: Volume.
- V_{EX}: Exchange flow.
- V_i: Volume for layer/compartment i.
- V_L: Volume for the lower layer.
- V_U: Volume for the upper layer.

- $V_{B,ST}$: Volume flow rate through the vent from the bottom space to the top space.
- $V_{T,ST}$: Volume flow rate through the vent from the top space to the bottom space.
- $V(z)$: Velocity of the mass flow at height z.
- Y_{LOL}: Limiting oxygen mass fraction.
- Y_{O_2}: Oxygen mass fraction.
- z: Height.
- Z_e: Interface height.
- Z_0: Flame height.
- z_1 : Lower end of an opening.
- z_2 : Upper end of an opening.
- z': Height from the neutral plane.
- z_1', z_2': Upper or lower end of the opening, or the neutral plane height.
- α: Flow coefficient.
- β: Coefficient for open/close tread.
- Γ: Perimeter of the shaft.
- γ: Ratio of specific heats.

- γ_{CO}: Mass ratio of the production of carbon monoxide to the carbon related products.
- $\gamma_{C/CRP}$: Mass fraction of the carbon in the CRP.
- γ_{Soot}: Mass ratio of the production of soot.
- ϵ: Emissivity.
- ρ_B: Density of the gases at the bottom of the vent.
- ρ_i: Density in layer/compartment i.
- ρ_L: Density in the lower layer.
- ρ_U: Density in the upper layer.
- ρ_T: Density of the gases at the top of the vent.
- $\triangle\rho$: Density difference of two compartment.
- σ: Stefan-Boltzman constant.
- χ_C: Mass fraction of carbon.
- χ_H: Mass fraction of hydrogen.
- χ_O: Mass fraction of oxygen.
- χ_{tox1},χ_{tox2}: Mass fractions of the first and second kinds of toxic species in the pyrolyzed fuel.
- ω: Constant.
- φ: Equivalence ratio of FO_P and FO_S.

Chapter 1

Introduction

Smoke generated by fires in buildings frequently creates a greater threat for occupants, than does heat. Reduced visibility and eye irritation caused by smoke make it impossible to see, so that an occupant in a building may be unable to locate escape routes and exits. Therefore, predicting smoke movement inside a building during a fire is very important. To do this, we seek to develop a hybrid computer-based model which combines the accuracy of a zone based model near the fire and the efficiency of a network based model sufficiently far away.

1.1 Background of Fire Safety Development

We begin with zone models. The zone models (Jones, 2001; Quintiere, 1995; Chow, 1996) were originally based on experimentally observed phenomena (Cooper,

et al., 1982). When there is a fire in a compartment, two layers of gas form in the fire and neighboring compartments due to thermal stratification, namely an upper hot smoke layer and a lower cool air layer. The zone model assumes that the gas temperature, as well as other smoke properties such as smoke and pollutant concentrations, are uniform within each layer. Smoke propagates from the fire source compartment to its neighboring compartments through the upper stratified hot smoke layer. The energy and mass transfer between the two zones and the surrounding rooms are then approximated. In the fire source compartment, the heat released by the fire causes a strong vertical flow (plume), which in turn plays a very important role in the smoke propagation. The characteristic smoke flow in the fire origin room subsequently affects the smoke propagation pattern in the neighboring compartments. Traditionally, the treatment of the fire source in the two-zone model is based on empirical formulas to estimate the fire plume size and smoke generation rate, and most of these empirical formulas are obtained from experiments under certain conditions.

As already discussed, the two-zone fire models can simulate smoke flow and temperatures resulting from building fires, but these simulations are limited to relatively few compartments due to computational complexity. It has been observed that these models often experience convergence failures with simulations over as few as six compartments. For the compartments far away from the fire origin, where two-zone models are not efficient to predict the conditions inside the compartments, the network model can be used to effectively model the scenario. The network model is based on the assumption that there is no smoke stratification and the properties of the gas are uniform throughout the compart-

ment. Due to this assumption, it is valid only for the spaces sufficiently remote from the fire-origin room where mixing is relatively complete. Computationally it is much simpler than the zone model. This simplicity makes it practical and efficient for the prediction of smoke spreading in high-rise buildings.

There has been no comprehensive model so far for the simulation of smoke transport in large, multi-compartmented buildings, except a recent approach developed by Floyd et al. (2005). For simulation of smoke flow in large buildings, an approximate method has been used that combines two separate models: (1) a zone fire model (such as FAST (Jones, 1985)) for simulation near the fire and (2) a network model (such as CONTAM (Walton, 1997; Dols, Denton, and Walton, 2000)) for simulation of smoke flow for locations remote from the fire. For example, the zone fire model, FAST, could be used to model the room of fire origin and a number of nearby rooms. This simulation provides temperature data that can be used as input data for a network simulation of the entire building. The simulations from this approximate method are recognized as crude at best, and in particular only the mass flow is determined over the entire building, the energy transfer is limited to the domain of the FAST simulation.

The aforementioned analysis indicates that it is necessary to develop a new model, which can give reliable prediction of smoke movement for building fires, especially for high-rise complex buildings, but stay within practical computer capability. A novel hybrid fire model to simulate the fire smoke propagation in a multi-storey building is presented in this thesis. This model comes from the

coupling of a two-zone and a network model which includes both mass and energy transfer. In the hybrid model, the two-zone model is used to model the fire smoke movement in the compartment with fire origin, as well as the fire smoke propagation in the compartments/corridors near the fire compartment where the hot smoke layer is well stratified and the smoke movement can be reasonably simulated based on the two-zone concept. Network modeling is employed for the simulation of smoke movement in the compartment far removed from the fire-origin where mixing is assumed relatively complete, thus properties are considered to be uniform in each compartment. Both mass flow and energy transfer are determined in the network model. The application of this model makes it possible to give a reasonable numerical simulation to the fire process in a whole high-rise building using standard PC computers.

The idea that fires could be studied numerically was probably first conceived at the start of the computer age and indeed the fundamental equations of fluid dynamics, heat transfer and combustion that are used in the more complex models today were first described over a century ago (see review in McGrattan et al., 2001). However, due to the innate complexity of fires and the large number of possible scenarios coupled with a limited amount of fire data and computer power, actual computer modeling of fires has only just come to fruition in the last 20 years (Mawhinney et al., 1994).

The two most prevalent approaches to fire modeling are: 1) probabilistic and 2) deterministic (Stroup, 1995). Probabilistic models make a risk based assessment of what could happen in a particular scenario based on experience and

past occurrences of fires. Deterministic models on the other hand provide a more rigorous mathematical approach to modeling based on physical laws (Kanury, 1987). Many phenomena in classical physics are explained using deterministic models. For example, Newton's laws of motion. The modeling of fire behavior, although vastly more complicated, naturally leads on from some of the classical physics equations such as those for fluid dynamics.

Deterministic fire models can range from quite simple correlations that utilize only a few equations to highly complex models requiring hours of computer time (Stroup, 1995). The purpose of the following is to provide an overview of deterministic fire modeling.

1.2 Zone Fire Modeling

Zone models are numerical tools commonly used for the evaluation of the temperature development of gases within a compartment during the course of a fire. Based on a limited number of hypotheses, they are easy to use and provide a good evaluation of the situation provided they are used within their field of application. Although zone models are a less sophisticated numerical fire model, they have been found to provide a good balance between accuracy and efficiency, thus are an essential tools in fire safety engineering applications. The main hypothesis in zone models is that the compartment is divided in zones in which the gas properties are uniform at any time.

Two-Zone Modeling:

When the size of the fire is small compared to the size of the compartment in which it develops, the hypothesis of uniform properties in the whole compartment is not valid. Another hypothesis is based on the observation that in such a case there is an accumulation of combustion products in a layer beneath the ceiling (upper layer), with a horizontal interface between this upper hot layer and the lower layer where the temperature of the gases remains much cooler. The main hypothesis of the two-zone model is that the temperature, gas density, internal energy and pressure are uniform in each layer, but different from one layer to another.

Conservation of mass, energy, and momentum are applied to each zone using algebraic representations and ordinary differential equations. As a result of the simulation, a gas temperature is given in each of the two layers, as well as the position of the interface, the information of the walls temperatures and flux through the openings. The thickness of the lower layer, which remains at relative cold temperature and contains no combustion products, is very important to judge the tenability of the compartment for the occupants. The two-zone models also have the capability to analyze more complex buildings where the compartment of fire origin exchanges mass and energy not only with the outside environment, but also with the other compartments in the building. This is of particular interest to analyze the propagation of smoke from the compartment of fire origin towards other adjacent compartments where it can also be a threat

for life.

The beginnings of the pre-flashover zone fire modeling can be traced to the mid-1970s with the publication of a description of the fundamental equations by Quintiere (1977). Based on these equations, the first zone fire model published was RFIRES by Pape et. al., (1981), followed shortly by the HARVARD model by Emmons and Milter (1985). The development of zone fire models was facilitated both by the advancement in the understanding of the basic physics of fire growth in a compartment and advances in, and availability of, mainframe computers. Following the publications of these two models a number of zone fire models for mainframe computers were introduced. In 1985 the first zone model, ASET-B (Available Safe Egress Time - BASIC), written specifically for the newly available IBM-compatible personal computers, was introduced by Walton (1985). Since that time numerous additional models have been introduced, and most of the models written for mainframe computers have been converted for use in personal computers.

Over the years, many zone models have been developed and studied. These models, in general, are designed to simulate buildings with a small number of compartments. The selection of a zone fire model for a particular application depends on a number of factors. While most zone models are based on the same fundamental principles, there is significant variation in their features. The decision to use a model should be based on an understanding of the assumptions and limitations for the particular model. In general, the more detailed the model

outputs, the more extensive the model inputs, and the greater the computer execution time required. When using any computer fire model, it is always a good idea to test the sensitivity of the model outputs to changes in model inputs. If small changes in model inputs result in large changes in model outputs, the user must exercise great care in selecting the input values.

ASET (Available Safe Egress Time) is a program for calculating the temperature and position of the hot upper smoke layer in a single room with closed doors and windows. ASET can be used to determine the time to the onset of hazardous conditions for both people and property. The required program inputs are the heat loss fractions, the height of the fuel above the floor, criteria for hazard and detection, the room ceiling height, the room floor area, a heat release rate, and (optional) species generation rate of the fire. The program outputs are the temperature, thickness, and (optional) species concentration of the hot upper smoke layer as a function of time, and the time to hazard and detection. ASET can examine multiple cases in a single run. ASET was written in FORTRAN by Cooper and Stroup (1982).

ASET-B (Available Safe Egress Time - BASIC) is a program for calculating the temperature and position of the hot smoke layer in a single room with closed doors and windows. ASET-B is a compact easy to run program which solves the same equations as ASET. The required program inputs are a heat loss fraction, the height of the fire, the room ceiling height, the room floor area, the maximum time for the simulation, and the rate of heat release of the fire. The program

outputs are the temperature and thickness of the hot smoke layer as a function of time. Different from ASET, ASET-B was written in BASIC by Walton (1985).

FIRST (FIRe Simulation Technique) is the direct descendant of the HARVARD program developed by Howard Emmons and Henri Mitler. The fire may be entered either as a user-specified time-dependent mass loss rate or in terms of fundamental properties of the fuel. In the latter case, the program will predict the fire growth rate by considering the changing oxygen concentration and smoke layer conditions in the room of fire origin. It can also predict the heating and possible ignition of up to three targets. The original fire and targets may also be user specified fires. The required program inputs are the geometrical data describing the rooms and openings, and the thermophysical properties of the ceiling, walls, burning fuel, and targets. The generation rate of soot must be specified, and the generation rates of other species may be specified as a yield of the pyrolysis rate. Among the program outputs are the temperature and thickness of, and species concentrations in, the hot upper layer and also in the cooler, lower layer in each compartment. Also given are wall surface temperatures, heat transfer rates and mass flow rates. The FIRST program was written in FORTRAN and is maintained by Mitler and Rockett (1987).

CCFM (Consolidated Compartment Fire Model version VENTS) is a two-layer zone-type compartment fire model. It simulates conditions due to user-specified fires in a multi-room, multi-level facility. The required inputs are a description of room geometry and vent characteristics (up to 9 rooms, 20 vents),

initial state of the inside and outside environments, and fire energy release rates as functions of time (up to 20 fires). If simulation of concentrations of products of combustion is desired, then product release rates must also be specified (up to three products). Vents can be simple openings between adjacent spaces (natural vents) or fan/duct forced ventilation systems between arbitrary pairs of spaces (forced vents). For forced vents, flow rates and direction can be user-specified or included in the simulation by accounting for user-specified fan and duct characteristics. Wind and stack effects can be taken into account. The program outputs for each room are pressure at the floor, layer interface height, upper/lower layer temperature and (optionally) product concentrations. CCFM (version VENTS) was written in FORTRAN by Cooper and Forney (1990).

The zone model JET is a two-zone, single compartment computer model designed to predict the plume centerline temperature, the ceiling jet temperature and the ceiling jet velocity produced by a single fire plume. The impact on the upper layer due to the presence of draft curtains, ceiling vents and thermal losses to the ceiling are included in the model. The unique feature of this model is that the characteristics of the ceiling jet depend on the depth of the hot layer. JET was written in FORTRAN by Davis (1999).

The CFAST (consolidated model of fire growth and smoke transport) is a upgrade of the FAST program (Jones, 1985) and incorporates numerical solution techniques originally implemented in the CCFM program. FAST is now the graphical interface program for CFAST. CFAST is a multi-room model that pre-

dicts fire and smoke movement within a structure resulting from a user-specified fire. CFAST version 4.0.1 can accommodate up to 30 compartments with multiple openings between compartments and to the outside. The required program inputs are the geometrical data describing the compartments and connections; the thermophysical properties of the ceiling, walls, and the floors; the fire as a rate of mass loss; and the generation rates of the products of combustion. The program outputs are the temperature, thickness of, and species concentration in the hot upper layer and the cooler lower layer in each compartment. Also given are the surface temperatures and heat transfer and mass flow rates. CFAST also includes mechanical ventilation, a ceiling jet algorithm, capability of multiple fires (up to 30), heat transfer to targets, detection and suppression systems, and a flame spread model. CFAST has been developed and used for many years, and many consider CFAST as a benchmark for two-zone modeling. We will compare solutions between our two-zone model and CFAST in chapter 4.

BRANZFIRE is a zone fire model for predicting the fire environment in an enclosure, resulting from a room-corner fire involving walls and ceilings. The zone fire model uses conservation equations based on those found in CFAST. BRANZFIRE predicts ignition, flame spread, and the resultant heat released by the wall and ceiling lining material subjected to a burning fire. The model considers upward flame spread on the walls and beneath the ceiling, lateral flame spread on the walls, and downward flame spread from the ceiling jet. Wall and ceiling flame spread properties are computed from cone calorimeter data. Program outputs include layer height, species concentrations, gas temperatures,

visibility, wall temperatures, and heat release rate. BRANZFIRE was written in Visual Basic by Wade (1999).

Zone model assumptions:

Assumptions have to be made in order to use the governing equations that are the base of the two-zone models. Many of these assumptions are based on observation from experimental tests and models. Below is a list of the major assumptions made in a two-zone model.

- Layers are assumed to be uniform throughout, which is valid provided the relative difference in temperature between layers is large.
- The fire plume acts as a pump of mass (smoke particles) and heat to the upper zone. However, the plume volume is assumed to be small compared to the upper and lower zones and so is negligible.
- The majority of the room contents are ignored; heat is lost to the room structure, but not the contents.
- The compartment gases in the upper and lower layers are treated as an ideal gas with a constant molecular weight.
- Exchange of mass at free boundaries is due to pressure differences caused by natural or forced convection.
- The pressure in the compartment is considered uniform in the energy equation.

- Fluid frictional effects at solid boundaries are ignored.
- All mass flows are driven by pressure and density differences that result from temperature differences and zone depths.

Inputs:

- Room geometry.
- Room construction (including all walls, floors and ceilings).
- Number of vents (or holes) and their sizes.
- Room furnishing characteristics.
- Heat release rate.
- Fire location and characteristics.

Outputs:

- Prediction of sprinkler and fire detector activation time.
- Time to flashover.
- Upper and lower layer temperature.
- Smoke layer height.
- Species yield.

Strengths:

- Established as a fire protection tool.
- Relatively easy to use and cheap on computer time; most models only take several minutes to compute.
- Can address multiple fires.
- Capable of modeling ventilation systems.

Limitations:

- Difficulty in getting convergence with even 5 or 6 compartments.
- Absence of a fire growth model.
- Cannot accurately take re-radiation into account from the surroundings.
- Heat release rate is not an output; tests must be done to quantify the size of fire adequate for the intended purposes.
- Many of the correlations are empirical in nature; some correlations may not fit the model, but still be used.
- Momentum is not explicitly considered in energy equations.
- Has no explicit ability to model radiological source terms.

With a brief review on the background of zone models, next we discuss several key aspects of a fire which are very important for the development of our two-zone model.

Plume Entrainment

Fire-induced buoyant plume entrainment is a very important factor in modeling fire growth and smoke spread in a building. A number of formulas can be found in the literature (Cetegen, et. al., 1984; Dembsey, et. al., 1995; Heskestad, 1995; McCaffrey, 1983; Zukoski, 1994). A widely accepted consensus on entrainment models for large fires in compartments does not yet exist. A review of existing models shows that they are based primarily on data from smaller fires (Dembsey, et. al., 1995; Zukoske, 1994).

Some full-scale standard room fire experiments at NIST indicated that McCaffrey's model (used by CFAST) gives the best agreement with the measured entrainment rates, although it does not account for the changing surrounding gas density (Dembsey, et al., 1995). In this model, both McCaffrey's and Heskestad's entrainment models have been used (McCaffrey, 1983; Heskestad, 1995). McCaffrey's equation is:

$$\frac{\dot{m}_e}{Q_c} = C_{E1} \left(\frac{Z_e}{Q_c^{2/5}} \right)^{C_{E2}}, \tag{1.1}$$

where

$\dot{m}_e$ is the plume entrainment rate,

Q_c is the convection heat release rate,

Z_e is the interface height.

Condition	C_{E1}	C_{E2}
$0 \leq \frac{Z_e}{Q_C^{2/5}} < 0.08$	0.011	0.566
$0.08 \leq \frac{Z_e}{Q_C^{2/5}} < 0.2$	0.026	0.909
$0.2 \leq \frac{Z_e}{Q_C^{2/5}}$	0.124	1.895

Table 1.1: Coefficients values for C_{E1} and C_{E2}

and C_{E1}, C_{E2} are constant coefficients in Table 1.1.

Heskestad's plumed equations are as follows:

$$Z_0 = 0.166 Q_C^{2/5}, \tag{1.2}$$

$$\dot{m}_e = \begin{cases} 0.0056 Q_C Z_e / Z_0 & \text{if } Z_e \leq Z_0, \\ \\ 0.071 Q_C^{1/3} Z_e^{5/3} + 0.0018 Q_C & \text{if } Z_e > Z_0. \end{cases} \tag{1.3}$$

If fires burn along the walls or in corners, plume entrainment rate will be restricted. The effects can be treated as follows (Mowrer & Williamson, 1987):

$$\dot{m}_e = f(Q_C, Z_e).$$

Then mass entrainment rate for wall and corner fires will be:

$$\dot{m}_e = f(\omega Q_C, Z_e)/\omega,$$

where for corner fire, ω is 4, for wall fire, ω is 2, and for center fire, ω is 1.

As the entrainment formula is an empirical relation based on experiments, its application is limited to the range of the experimental data. Mowrer and Williamson have reported that for heat release rates ranges from 50 to 1000 KW, the mass entrainment rates for center, wall, and corner fires are in the range of (0.64 - 1.06), (0.48 - 0.85), and (0.35 - 0.67) kg/s, respectively (Mowrer & Williamson, 1987). To use equations (1.2) and (1.3) outside these ranges, it is necessary to limit the maximum entrainment rate based on energy balance:

$$\dot{m}_e \leq \frac{Q_C}{C_p(T_I - T_L)} - \dot{m}_{PF}, \tag{1.4}$$

where T_I is assumed to be the interface temperature, T_L is the lower temperature of the room, $\dot{m}_{PF}$ is the mass pyrolysis rate. Equation (1.4) implies that the averaged plume temperature at the interface should be greater than T_I. In this model, T_I is obtained based on Cooper's N percent rule (Peacock, et. al., 1991; Cooper, et. al., 1982).

Combustion Model

Heat Release Rate:

The heat release rate in unconstrained combustion can be obtained by:

$$Q_N = \dot{m}_{PF}(\Delta H)_F,$$

where $(\Delta H)_F$ is the effective heat of combustion per unit kilogram fuel in open

air. Following the oxygen consumption principle, the oxygen consumption rate can be obtained using (Huggert, 1980; Parker, 1984):

$$\dot{m}_{O_2} = \frac{Q_N}{(\Delta H)_O},$$

where, $(\Delta H)_O$ is the heat of combustion per unit kilogram oxygen. For complex fuels, it could be taken as 13.2 MJ/kg, while for simple chemical formula fuels, it could be obtained from the value of heat of combustion per unit kilogram fuel.

The stoichiometric fuel to oxygen ratio, FO_S, is:

$$FO_S = \frac{(\Delta H)_O}{(\Delta H)_F},$$

here $(\Delta H)_F$ is the heat of combustion per unit kilogram fuel. The actual fuel to oxygen ratio in the fire plume is:

$$FO_P = \frac{\dot{m}_{PF}}{\dot{m}_e Y_{O_2}},$$

where $\dot{m}_e$ is the mass entrainment rate of the plume, and Y_{O_2} is the oxygen mass fraction. Thus the equivalence ratio, φ, is:

$$\varphi = \frac{FO_P}{FO_S} = \frac{(\Delta H)_F \dot{m}_{PF}}{(\Delta H)_O \dot{m}_e Y_{O_2}}.$$

The actual heat release rate is considered to be related to φ as follows:

$$Q = f(\varphi)\dot{m}_{PF}(\Delta H)_F.$$

Here $f(\varphi)$ can be obtained from the following simple relation used by CFAST (Peacock, et. al., 1993):

$$f(\varphi) = \frac{1}{\max(\varphi, 1)}.$$

The fuel rich flammability is given by a limiting oxygen mass or volume fraction. In order to make the calculation smooth near the fuel rich limit, following CFAST, a limiting coefficient C_{LOL} is introduced (Peacock, et. al., 1993):

$$C_{LOL} = \frac{\tanh(800(Y_{O_2} - Y_{LOL}) - 4) + 1}{2},$$

and

$$Q = \frac{Q_N C_{LOL}}{\max(\varphi, 1)},$$

where Y_{LOL} is the limiting oxygen mass fraction (Morehart, 1991).

The mass of total burnt fuel and consumed oxygen is given as:

$$\dot{m}_{BF} = \frac{Q}{(\Delta H)_F},$$

$$\dot{m}_{O_2} = \frac{Q}{(\Delta H)_O}.$$

Combustion Chemistry.

In this model, combustion chemistry is considered as follows:

$$\begin{aligned} & m_{PF}(m_{PFmin} + m_{CHO}) + m_{O_2} \\ \rightarrow\ & m_{CRP}(m_{CO_2} + m_{CO} + m_{Soot}) + m_{H_2O} + m_{PFmin} + m_{TUF}, \end{aligned} \tag{1.5}$$

where m_{PF} is the mass of fuel pyrolysis, composed of two parts, m_{PFmin} and m_{CHO}.

m_{PFmin} is assumed to be some harmful species, such as HC1 and HCN, whose mass is much less than m_{PF} and will not further be involved in the combustion process. Thus m_{PFmin} from m_{PF} on the left side of (1.5) directly goes into its right side. In this model, m_{PFmin} can be composed of as many as three kinds of toxic species: m_{tox1}, m_{tox2}, and m_{tox3}. m_{CHO} is the mass of the fuel pyrolysis excluding m_{PFmin}, it is assumed to be composed of carbon, hydrogen and oxygen. The mass production of CO_2, CO and soot are combined into one new term m_{CRP}, carbon-related products, and soot is assumed to be carbon only.

m_{TUF} is the mass production of total unburned fuel, which is assumed to have the same element composition as m_{CHO}.

The following presents the calculation formulas of the combustion chemistry. The composition of the pyrolyzed fuel is defined by the following five mass ratios, which are input by the user of the model.

$$\chi_C = \frac{m_C}{m_{PF}},$$

$$\chi_H = \frac{m_H}{m_{PF}},$$

$$\chi_O = \frac{m_O}{m_{PF}},$$

$$\chi_{tox1} = \frac{m_{tox1}}{m_{PF}},$$

$$\chi_{tox2} = \frac{m_{tox2}}{m_{PF}},$$

where χ_C, χ_H, χ_O, χ_{tox1} and χ_{tox2} are mass fractions of carbon, hydrogen, oxygen, and the first and second kinds of toxic species in the pyrolyzed fuel, respectively.

Based on the above five mass ratios, the toxic species production is then computed using:

$$m_{PFmin} = [1 - (\chi_C + \chi_H + \chi_O)]m_{PF},$$

$$m_{tox1} = \chi_{tox1} m_{PF},$$

$$m_{tox2} = \chi_{tox2} m_{PF},$$

$$m_{tox3} = m_{PFmin} - (m_{tox1} + m_{tox2}).$$

The mass ratios of the production of soot and carbon monoxide to the carbon related products, γ_{CO} and γ_{Soot}, are also defined by the user:

$$\gamma_{CO} = \frac{m_{CO}}{m_{CRP}},$$

$$\gamma_{Soot} = \frac{m_{Soot}}{m_{CRP}}.$$

Then the production of the carbon related products of combustion can be obtained from:

$$m_{CRP} = \frac{\chi_C m_{BF}}{\gamma_{C/CRP}}, \tag{1.6}$$

where, $\gamma_{C/CRP}$ is the mass fraction of the carbon in the CRP as follows:

$$\gamma_{C/CRP} = \frac{3}{11} + \frac{12}{77}\gamma_{CO} + \frac{8}{11}\gamma_{Soot}. \tag{1.7}$$

From the production of the carbon related products m_{CRP}, the production of soot, carbon monoxide and carbon dioxide can be obtained as follows:

$$m_{Soot} = \gamma_{Soot} m_{CRP},$$

$$m_{CO} = \gamma_{CO} m_{CRP},$$

$$m_{CO_2} = (1 - \gamma_{Soot} - \gamma_{CO}) m_{CRP}.$$

Water production m_{H_2O} and the total unburned fuel m_{TUF} can be obtained as follows:

$$m_{H_2O} = 9\chi_H m_{BF},$$

$$m_{TUF} = (\chi_C + \chi_H + \chi_O)(m_{PF} - m_{BF}).$$

In this model, m_{BF} is assumed to have the same element composition as m_{PF}, and all the hydrogen in the burned fuel is changed into water.

Calculation of $(\Delta H)_O$ and $(\Delta H)_F$:

For a chemical reaction, there is a fixed relationship between the heat of combustion per unit mass of burned fuel $(\Delta H)_F$ and per unit mass of consumed oxygen $(\Delta H)_O$. For a fixed reaction with a given $(\Delta H)_F$, $(\Delta H)_O$ should be computed accordingly to ensure oxygen balance.

The relationship of $(\Delta H)_F$ and $(\Delta H)_O$ can be derived from the following combustion relation without the unburned production ($m_{PF} = m_{BF}$):

$$m_{PF}(m_{PFmin} + m_{PFmain}) + m_{O_2} \rightarrow m_{PFmin} + m_{CRP} + m_{H_2O}.$$

By balancing the mass of oxygen in the above relation, the following equation can be obtained:

$$\chi_O m_{PF} + m_{O_2} = m_{CRP}(1 - \gamma_{C/CRP}) + \frac{8}{9} m_{H_2O}.$$

Substituting Equation (1.6) and (1.7) into the above equation gives:

$$m_{O_2} = \left(\frac{\chi_C}{\gamma_{C/CRP}} (1 - \gamma_{C/CRP}) + 8\chi_H - \chi_O \right) m_{PF}.$$

Based on the definition of $(\Delta H)_F$ and $(\Delta H)_O$, we have:

$$(\Delta H)_O m_{O_2} = (\Delta H)_F m_{PF}.$$

Then we can get:

$$(\Delta H)_O = \frac{(\Delta H)_F}{\frac{\chi_C}{\gamma_{C/CRP}} - \chi_C + 8\chi_H - \chi_O}.$$

In this model, $(\Delta H)_F$ is the user input. If $(\Delta H)_F$ is input as zero, then $(\Delta H)_O$ is taken as 13.2 MJ/Kg.

In summary, by specifying the mass pyrolysis rate $\dot{m}_{PF}$, the various mass ratios χ_C, χ_H, χ_O, χ_{tox1}, χ_{tox2}, χ_{CO}, χ_{Soot}, and the heat of combustion per unit mass of fuel for the specified chemical reaction $(\Delta H)_F$, the heat release rate and species production and consumption rates can be calculated.

1.3 Network Fire Modeling

Network models form the basis of most computer simulations of airflow and pollutant transport in buildings. Network models have been developed by numerous researchers including Butcher et al. (1969), Barrett and Locklin (1969), Sander and Tamura (1973), Wakamatsu (1977), Yoshida et al. (1979), Evers and Waterhouse (1978), Klote (1982) and Walton (1989). The best network models can simulate smoke flow in extremely large buildings, but have major limitations concerning temperature prediction.

The most advanced and sophisticated network model is CONTAM (Walton 1997; Dols, Denton, and Walton 2000) which can simulate flow inside buildings

consisting of thousands of compartments including stack effect, wind effect and forced ventilation. CONTAM was originally developed for indoor air quality applications, but it has become the most extensively used network program for smoke control analysis. It is used to predict conditions in the spaces far remote from the fire room, where temperatures are near ambient and layering does not occur. We will compare our network model with CONTAM using a three-storey 12-room building case in chapter 4.

COMIS (Feustel 1999), is a recent development in inter-zonal air flow modeling (Feustel 1996). Because of its modular structure, COMIS has greater capability to simulate buildings than do earlier multi-zone air-flow models. COMIS can be used as a stand-alone-model with input and output features or as an air-flow module for thermal building simulation programs. It can also serve as a module library, that could be used by authors of similar models. COMIS grew from the work of an International Energy Agency's (IEA) expert group that began addressing multi-zone air-flow modeling in 1990. The objective of this group was to study physical phenomena causing air flow and pollutant transport (e.g., moisture) in multi-zone buildings and to develop modules to be integrated in a multi-zone air-flow modeling system. Because it was developed by an international group of scientists under the aegis of the IEA, COMIS has the potential for immediate adoption in a number of countries and may therefore become a standard in multi-zone air flow modeling. So far, more than 200 copies of the program are being used in more than 15 countries. Modules being used in COMIS include air-flow equations for large vertical openings, single-sided ventilation,

and different opening situations for various window constructions. Special emphasis was given to providing data necessary to use the system (e.g., calculation of wind pressure distribution).

In these types of models, the structure is idealized as a network of well-mixed spaces, or zones of uniform properties (temperature, contaminant concentration, etc.). These zones are connected via mathematical flow paths. Flow path models range from simple cracks, to windows and doors, to active elements such as fans. By contrast, the programs provide only one zone model, which represents a well-mixed space with simple hydrostatic pressure variations. A simulation predicts the systems behavior based on the interactions of the assembled components. Simultaneous mass balance is used to determine pressure.

Network modeling adopts a numerical approach. Governing equations are defined across each flow path and physical properties are iteratively calculated until the solution converges. Following are typical calculation steps in the nodal network model (Liddament, 1996):

- Develop the flow equations.
- Develop a flow path network and define the pressure/air flow characteristics of each flow path or opening.
- Determine the strength of driving forces acting across each path.
- Incorporate mechanical ventilation into the flow network.

- Solve for mass flow balance between incoming and outgoing air.

Network model assumptions:

- Decouple the air flow problem from the thermal problem by assuming that the temperatures remain fixed.
- Also decouple the airflow and pollutant transport problems, by assuming the amount of pollutant in a space does not affect the airflows.

Features:

- Used for the calculation of air flows, air change rates, and contaminant transport in building.
- Can assess the adequacy of ventilation rates, the variation in ventilation rates, and the distribution of ventilation air.
- Can be used to determine the indoor air quality performance of a building and investigate the various design decisions.
- Examines the effects of varying equipment efficiencies.
- Performs exposure analysis for occupants of structure.
- Models infiltration of outdoor contaminant and transport of indoor sources of contaminants.

- Capable of considering the effects of stack effect, wind, smoke temperature, and HVAC systems of smoke movement within a building.

Inputs:

- Building idealization.
- Schematic representation.
- Defining building components.

Strengths:

- High computational speed.
- Low computer memory requirements.
- Quick convergence.

Limitations:

- Network model does not consider heat transfer and energy-balance, and thus the temperature of each zone cannot be predicted, but has to be input as a constant value.
- Driving forces need to be quantified and all openings in the structure of the building accounted for accurately.

- The assumption that air and pollutant in each zone is uniformly mixed is not necessarily true in reality.

1.4 General Discussion on Flow through Vents

In this section, we discuss flow through two types of vents: horizontal flow through a vertical vent, and vertical flow through a horizontal ceiling vent.

1.4.1 Horizontal Flow through a Vertical Vent

The flow through normal vents such as windows and doors is governed by the pressure difference across a vent, and the discontinuity in heights of the layers (in case of two-zone compartment), in addition to the geometry of the opening. A momentum equation for the zone boundaries is not solved directly. Instead momentum transfer at the zone boundaries is included by using an integrated form of Euler's equation, namely Bernoulli's solution for the velocity equation. This solution is augmented for restricted openings by using flow coefficients to allow for constriction from finite size doors. The flow (or orifice) coefficient is an empirical term which addresses the problem of constriction of velocity streamlines at an orifice.

Bernoulli's equation is the integral of the Euler's equation and applies to general initial and final velocities and pressures. The implication of using this equation for a zone model is that the initial velocity in the doorway is the quantity sought, and the final velocity in the target compartment vanishes. That is, the flow velocity vanishes where the final pressure is measured. Thus, the pressure at a stagnation point is used. This is consistent with the concept of uniform zones which are completely mixed and have no internal flow. The following discusses the details of the horizontal mass flow through a vertical vent.

Letting $P_i(0)$ and $P_j(0)$ be the pressure of the compartment on each side of the opening i and j at a reference level, respectively, the pressure at arbitrary height z from the reference level $P_i(z)$ and $P_j(z)$ can be given as (Tanaka & Yamada, 2004):

$$P_i(z) = P_i(0) - \rho_i g z \quad (z \leq H),$$

$$P_j(z) = P_j(0) - \rho_j g z \quad (z \leq H),$$

where ρ_i and ρ_j are the densities of the gases in the compartments i and j, respectively, and g is the acceleration due to gravity.

Detailed Calculation of Mass Flow Rates.

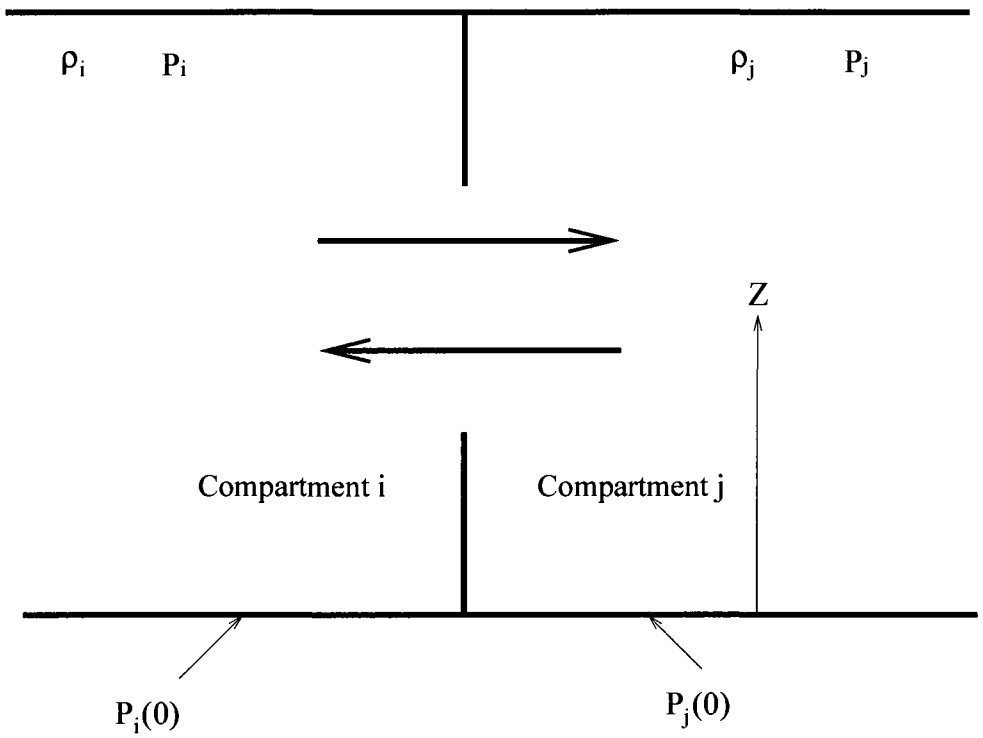

Figure 1.1: Flow through an opening

The difference of pressure at height, z, from the reference level is as follows:

$$P_i(z) - P_j(z) = (P_i(0) - \rho_i g z) - (P_j(0) - \rho_j g z).$$

We can rewrite the above equation as:

$$\Delta P(z) = \Delta P(0) - \Delta \rho g z,$$

where $\Delta P(z) = P_i(z) - P_j(z)$, $\Delta P(0) = P_i(0) - P_j(0)$, and $\Delta \rho = \rho_i - \rho_j$.

It is assumed that the velocity of the gas flow as a function of height, z, is given by the following orifice equation (Bernoulli's equation):

$$V(z) = \alpha \sqrt{\frac{2[P_i(z) - P_j(z)]}{\rho_i}},$$

where α is the discharge coefficient, ρ_i is the density of the gas (upstream) going through the opening.

The mass flow from compartment i to compartment j through an opening is given by:

$$\dot{m}_{ij} = B \int_{z_1}^{z_2} \rho_i V(z) dz,$$

$$\Rightarrow \quad \dot{m}_{ij} = \alpha B \int_{z_1}^{z_2} \rho_i \sqrt{\frac{2|\Delta P(0) - \Delta \rho g z|}{\rho_i}} dz,$$

where B is the width of the opening, and the heights z_1 and z_2 in the above equation are the lower and upper ends of the opening.

Unidirectional Flow.

If the densities of both compartments are equal, $\Delta\rho$ would become zero. In this particular case, flow occurs only due to the pressure difference (with no changes in temperature). The above mass flow equation becomes:

$$\dot{m}_{ij} = \alpha B \int_{z_1}^{z_2} \rho_i \sqrt{\frac{2|\Delta P(0)|}{\rho_i}} dz,$$

$$\Rightarrow \quad \dot{m}_{ij} = \alpha B \sqrt{2\rho_i |\Delta P(0)|}\, |z_2 - z_1| .$$

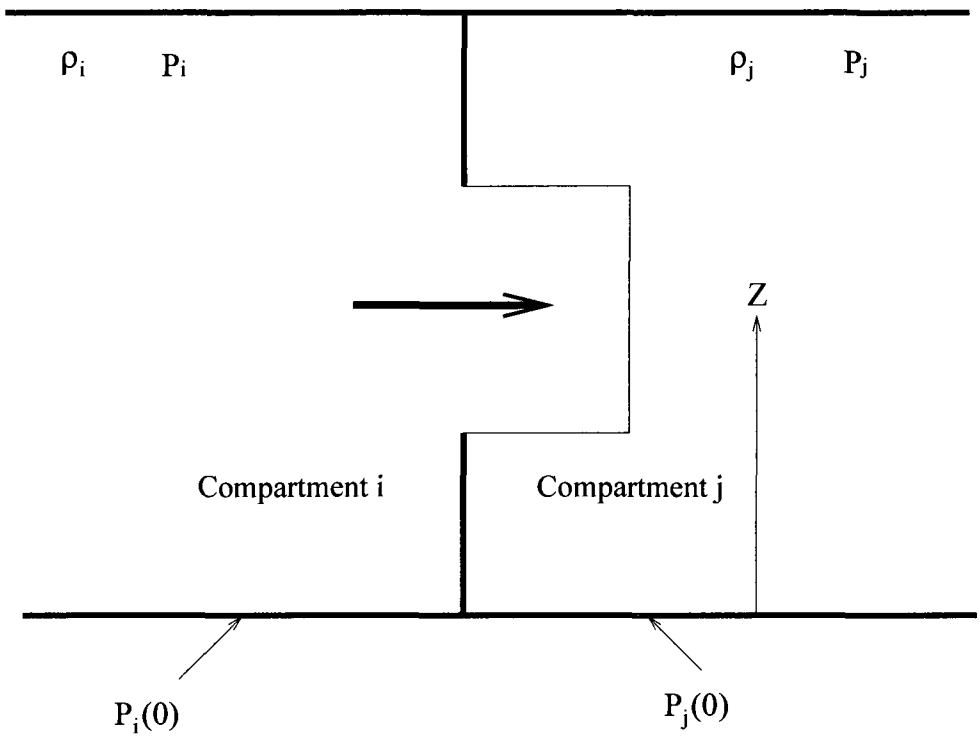

Figure 1.2: Unidirectional flow through an opening (assuming $P_i > P_j$)

Bi-directional Flow.

As discussed above, the pressure difference at height, z, from the reference level is given as follows:

$$\Delta P(z) = \Delta P(0) - \Delta \rho g z.$$

If the densities of the gases in the compartments are not equal, the pressure difference at a certain height would become zero. This plane with zero pressure difference is called Neutral Plane.

By putting $\Delta P(z) = 0$ in the above equation, the neutral plane height N_{ss} can be obtained as follows:

$$N_{ss} = \frac{\Delta P(0)}{\Delta \rho g}.$$

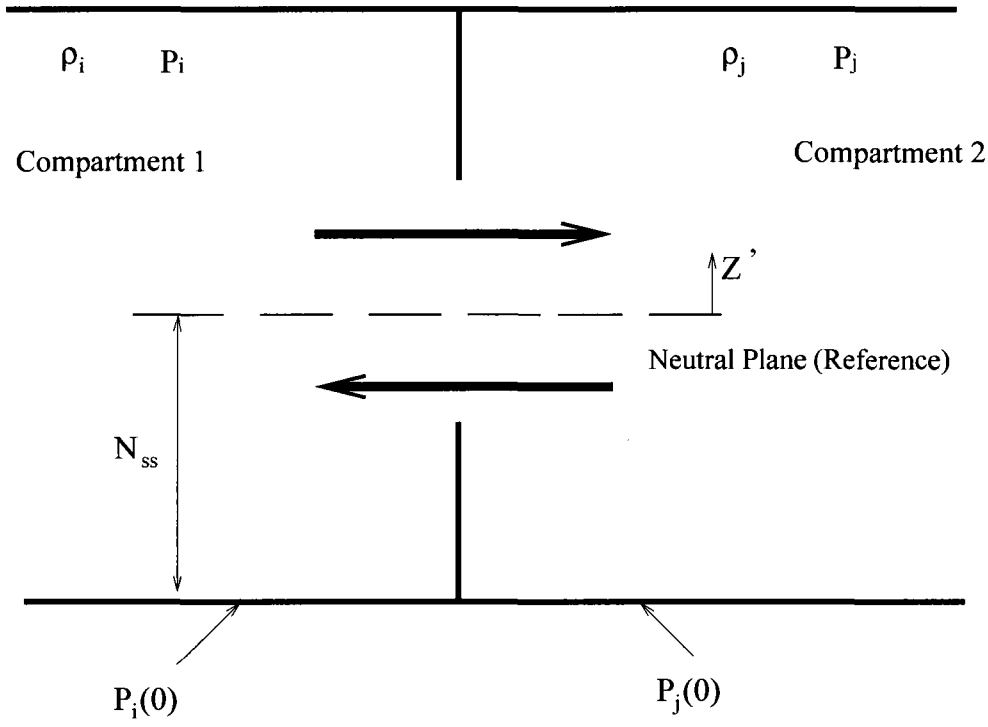

Figure 1.3: Bi-directional flow through an opening (assuming $\rho_i < \rho_j$ and N_{ss} is between the sill and soffit of the opening)

Now let the height of the neutral plane be the reference level and define z' be the height from that level, the pressure difference at height z' is simply given as:

$$\Delta P(z') = P_i(z') - P_j(z') = -(\rho_i - \rho_j)gz'.$$

Mass flow can be calculated as follows:

$$\dot{m}_{ij} = B \int_{z_1'}^{z_2'} \rho_i V(z') dz',$$

$$\Rightarrow \dot{m}_{ij} = \alpha B \int_{z_1'}^{z_2'} \sqrt{2g\rho_i|\Delta\rho|}(z')^{1/2} dz',$$

$$\Rightarrow \dot{m}_{ij} = \frac{2}{3}\alpha B \sqrt{2g\rho_i|\Delta\rho|}\left||z_2'|^{3/2} - |z_1'|^{3/2}\right|.$$

The heights z_1' and z_2' in the above equations can be either of the upper and lower ends of the openings, or the neutral plane height.

1.4.2 Vertical Flow through a Horizontal Ceiling Vent

Flow through a ceiling or floor vent can be more complicated than through door or window vents. The simplest form is uni-directional flow, driven solely by a pressure difference. This is analogous to flow in the horizontal direction driven by a piston effect of expanding gases. Once again, it can be calculated based on Bernoulli's equation. However, in general we deal with more complex situations that must be modeled in order to have a proper understanding of smoke movement. The first is an occurrence of puffing. When a fire exists in a compartment in which there is only one hole in the ceiling, the fire will burn until the oxygen has been depleted, pushing gas out the hole. Eventually the fire will die down.

At this point ambient air will rush back in, enable combustion to increase, and the process will be repeated. Combustion is thus tightly coupled to the flow. The other case is exchange flow which occurs when the fluid configuration across the vent is unstable (such as a hotter gas layer underneath a cooler gas layer). Both of these pressure regimes require a calculation of the onset of the flow reversal mechanism.

Normally a non-zero cross-vent pressure difference tends to drive unidirectional flow from the higher to the lower pressure side. An unstable fluid density configuration occurs when the pressure alone would dictate stable stratification, but the fluid densities are reversed. That is, the hotter gas is underneath the cooler gas. Flow induced by such an unstable fluid density configuration tends to lead to bi-directional flow, with the fluid in the lower compartment rising into the upper compartment. This situation might arise in real fire if the room of origin suddenly had a hole punched in the ceiling. No pretense is made of being able to do this instability calculation analytically. Cooper's algorithm (Cooper, 1989; Cooper, 1995; Cooper, 1997) is used for computing mass flow through ceiling and floor vents.

Standard Vent Flow Model.

It is assumed that in each space, near the vent elevation, but away from the vent flow itself, the environment is relatively quiescent with pressure well-

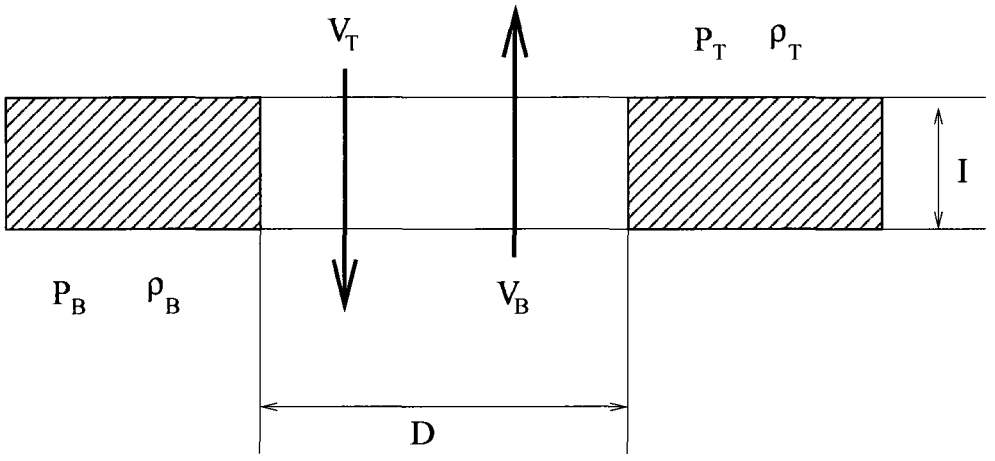

Figure 1.4: Basic horizontal-vent (ceiling vent) configuration model

approximated by the uniform pressure field which would be derived from hydrostatic momentum considerations. This assumption would be satisfied typically if the area of the vent is small compared to the plane area of either the upper or lower space. The two spaces connected by the vent are designated as the top and bottom space. The environment in each of the two spaces as shown in Figure 1.4 is known. The properties of the environment which are critical in the determination of the characteristics of the flow through the horizontal vent are the densities and the pressures at the top and bottom of the vent.

If the density of the gases at the top of the vent is greater than that at bottom ($\rho_T > \rho_B$), which occurs when the vent separates a relatively high temperature, low density environment at the bottom from a relatively cool, but high density environment at the top, then, according to the standard vent flow model, the flow through the vent for different values of ΔP is given in Table 1.2.

Condition	$V_{B,ST}$	$V_{T,ST}$
$\Delta P > 0$	$C_D A_v \sqrt{\lvert 2\Delta P/\rho_B \rvert}$	0
$\Delta P = 0$	0	0
$\Delta P < 0$	0	$C_D A_v \sqrt{\lvert 2\Delta P/\rho_T \rvert}$

Table 1.2: Volume flow rates between top and bottom space

For arbitrary,

$$\Delta\rho = \rho_T - \rho_B,$$

$$\Delta P = P_B - P_T.$$

In Table 1.2, $V_{B,ST}$ and $V_{T,ST}$ are the volume-flow-rates through the vent from the bottom space to the top space and from the top space to the bottom space, respectively, A_v, is the vent area, and C_D is the flow coefficient. It is noted that the standard model always yields unidirectional flow through the vent, where the flow direction is determined by the sign of ΔP, i.e., $V_{B,ST}$ and $V_{T,ST}$ are never both non-zero.

The above flow description seems reasonable, except for one problem which is the prediction of a state of stable hydrostatic equilibrium corresponding to a zero exchange flow when $\Delta P = 0$. The prediction is not realistic. Indeed, the hydrostatic state associated with the assumed configuration is not one of stable equilibrium and non-zero, time-dependent, exchange flows between the space are to be expected. To address this we introduce an extra exchange flow.

Exchange Flow: Since the standard vent-flow model is not generally adequate, it is assumed that the correct vent flow, $V_{B,ST}$ and $V_{T,ST}$, can be predicted by a sum of the standard model flow components on the above table and an exchange-flow component, V_{EX}, to be determined. Thus,

$$V_T = V_{T,ST} + V_{EX},$$

$$V_B = V_{B,ST} + V_{EX}.$$

When the density configuration does not lead to an unstable hydrostatic configuration, the standard model is valid. In particular, $V_{EX} = 0$ for arbitrary ΔP if $\rho_T \leq \rho_B$.

For generalized calculation of mass/volume flow through a ceiling/floor vent, see reviews in (Cooper, 1989).

Stair Shaft Flow

When dealing with multi-storey buildings, it is important to compute the mass or volume flow rate through a stair shaft, because a stair shaft is the main path of smoke spread from floor to floor. Achakji and Tamura conducted research on pressure drop characteristics of typical stair shafts in high-rise buildings (Achakji and Tamura, 1994). It was found that pressure drop through a stair shaft can be represented by a pressure loss across an equivalent horizontal orifice located between floors of a frictionless stair shaft.

Based on Achakji and Tamura's experimental data, a correlation for calculating the area of the effective orifice was obtained and used in CONTAM, a model used to analyze contaminant migration in a building (Walton, 1997). This correlation is as follows:

For open treads:

$$Ae_i = 0.089 h_i A_S (1.0 - 0.14\sqrt{d_i}). \tag{1.8}$$

For closed treads:

$$Ae_i = 0.083 h_i A_S (1.0 - 0.24\sqrt{d_i}). \tag{1.9}$$

As shown in Figure 1.5, the parameters in the above two equations are as follows: Ae_i is the effective orifice area on the i^{th} floor, h_i is the height of the shaft between the i^{th} floor and $(i-1)^{\text{th}}$ floor, d_i is the density of people on the stairs between the i^{th} and $(i-1)^{\text{th}}$ floor, and A_S is the cross-sectional area of the stair shaft.

It was found that there is a problem in the two equations with the relationship between Ae_i and h_i. Following equations (1.8) and (1.9), the higher h_i is, the larger the area Ae_i is. This is contradictory to the real physical laws of fluid flow. As h_i represents the length of the stair shaft, it is expected that increasing h_i will increase friction and decrease the effective area Ae_i. After carefully re-investigating the original paper (Achakji and Tamura, 1994) referenced by

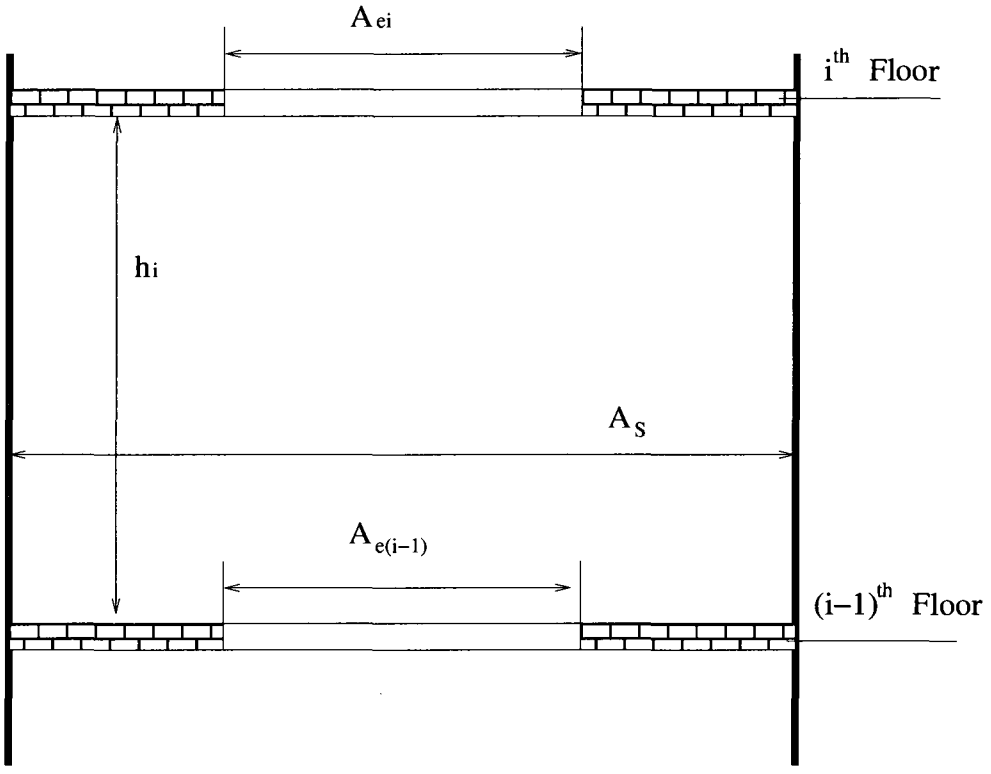

Figure 1.5: Schematic of an effective ceiling vent for a stair shaft

CONTAM, it was found that the following equation provides a more accurate representation:

$$\frac{Ae_i}{A_S} = \frac{1}{C_{CV}\left(k\frac{h_i}{D_e}\right)^{1/2}}, \tag{1.10}$$

where C_{CV} is the coefficient of discharge, taken as 0.6 in reference (Achakji and Tamura, 1994); k is the friction pressure loss coefficient; D_e is the equivalent diameter, which can be calculated by the stair shaft cross-sectional area A_S and the perimeter of the shaft Γ as follows:

$$D_e = \frac{4A_S}{\Gamma}.$$

Equation (1.10), however does not include the effect of the density of people d_i. To account for this, the approach used in Equations (1.8) and (1.9) is followed, resulting in the following equation that is used in the model:

$$\frac{Ae_i}{A_S} = \frac{1.0 - \beta\sqrt{d_i}}{C_{CV}\left(k\frac{h_i}{D_e}\right)^{1/2}}, \tag{1.11}$$

where β is taken as 0.14 for open tread case, 0.24 for closed tread case. According to reference (Achakji and Tamura, 1994), k is taken as 29 for open tread case and 32 for closed tread case. In the model, after the equivalent Ae_i is obtained from Equation (1.11), Cooper's (Cooper, 1996) ceiling vent flow model is used to calculate the volumetric flow rate through the ceiling vent.

Chapter 2

Description of the Hybrid Model

In previous chapter, we gave a brief review on some of the two-zone and the network models. Our hybrid model is different from those existing fire and smoke models, such that 1). our hybrid model combines a two-zone model and a network model; 2). our network model takes account of both mass and energy transfer/exchange. In this chapter, we present a derivation of the equations for the hybrid model, which would help the model user to understand the underlying theory behind the model implementation and thus be able to assess the appropriateness of the model to specific problems.

2.1 Governing Equations for Two-Zone Modeling

The modeling equations used in this model (similar to CFAST) take the mathematical form of an initial value problem for a system of ordinary differential equations. These equations are based on the conservation of mass, the conservation of energy (equivalently the first law of thermodynamics), and the ideal gas law. These equations predict, as functions of time, quantities such as pressure, layer height and temperatures in the two layers.

Many formulations based upon these assumptions can be derived. One formulation can be converted into another using the definitions of density, internal energy and the ideal gas law. Though equivalent analytically, these formulations differ in their numerical properties. Each formulation can be expressed in terms of mass and enthalpy flow. These rates represent the exchange of mass and enthalpy between zones due to physical phenomena such as plumes, natural and forced ventilation, convective and radiative heat transfer, and so on (Jones et al., 2005). For example, a vent exchanges mass and enthalpy between zones in connected rooms, a fire plume typically adds heat to the upper layer and transfers entrained mass and enthalpy from the lower to the upper layer, and convection transfers enthalpy from the gas layers to the surrounding walls.

A compartment is divided into two control volumes, a relatively hot upper layer and a relatively cool lower layer. The gas in each layer has attributes of

mass, internal energy, density, temperature, and volume denoted respectively by m_i, E_i, ρ_i, T_i, V_i and where $i = L$ for the lower layer and $i = U$ for the upper layer. The compartment as a whole has the attribute of pressure P. These eleven variables are related by means of the following seven constraints (density, internal energy and the ideal gas law twice, once for each layer) (Fu, et al., 2002):

$$\rho_i = \frac{m_i}{V_i}, \quad \text{(density)} \tag{2.1}$$

$$E_i = C_v m_i T_i, \quad \text{(internal energy)} \tag{2.2}$$

$$P = \rho_i R T_i, \quad \text{(ideal gas law)} \tag{2.3}$$

$$V = V_L + V_U. \quad \text{(total volume)} \tag{2.4}$$

The specific heat at constant volume and at constant pressure C_v and C_p, the universal gas constant, R, and the ratio of specific heats, γ, are related by:

$$\gamma = \frac{C_p}{C_v},$$

and

$$R = C_p - C_v.$$

Four additional equations obtained from conservation of mass and energy for each layer are required to complete the equation set. The differential equations

for the rate of change of mass in each layer are:

$$\frac{dm_L}{dt} = \dot{m}_L,$$

$$\frac{dm_U}{dt} = \dot{m}_U,$$

where $\dot{m}_L$ and $\dot{m}_U$ are the net mass gain rate of the lower and upper layer, respectively, by mass flow across the boundary.

The first law of thermodynamics states that the rate of increase of internal energy plus the rate at which the layer does work by expansion is equal to the rate at which enthalpy is added to the gas. In differential form this is:

$$\frac{dE_i}{dt} + P\frac{dV_i}{dt} = \dot{h}_i, \tag{2.5}$$

where C_p is assumed constant in enthalpy term,

$$\dot{h}_i = C_p \dot{m}_i T_i + \dot{E}_{hi}, \tag{2.6}$$

where the first term on the right-hand side of the equation represents the rate of net enthalpy gain of layer i by mass flow across the boundary, and the second term is the rate of net heat gain of layer i by heat transfer or combustion.

A differential equation for pressure can be derived by adding the upper and lower layer of equation (2.5), noting that $dV_U/dt = -dV_L/dt$, and substituting the differential form of equation(2.2) to get:

$$\frac{dP}{dt} = \frac{\gamma - 1}{V}(\dot{h}_L + \dot{h}_U). \tag{2.7}$$

Differential equations for the layer volumes can be obtained by substituting the differential form of equation(2.2) into equation (2.5) to obtain:

$$\frac{dV_i}{dt} = \frac{1}{\gamma P}\left[(\gamma - 1)\dot{h}_i - V_i\frac{dP}{dt}\right]. \tag{2.8}$$

Equation(2.5) can be rewritten using equation (2.8) to eliminate dV_i/dt to obtain:

$$\frac{dE_i}{dt} = \frac{1}{\gamma}\left(\dot{h}_i + V_i\frac{dP}{dt}\right). \tag{2.9}$$

A differential equation for the density can be derived by noting $\frac{d\rho_i}{dt} = \frac{d}{dt}(\frac{m_i}{V_i})$ and using equation (2.8) to eliminate dV_i/dt to obtain:

$$\frac{d\rho_i}{dt} = \frac{1}{C_p T_i V_i}\left[(\dot{h}_i - C_p\dot{m}_i T_i) - \frac{V_i}{\gamma - 1}\frac{dP}{dt}\right]. \tag{2.10}$$

Temperature equations can be obtained from the equation of state by computing $\frac{dT_i}{dt} = \frac{d}{dt}(\frac{P}{\rho_i R})$ and using equation (2.10) to eliminate $d\rho_i/dt$ to obtain:

$$\frac{dT_i}{dt} = \frac{1}{C_p \rho_i V_i}\left[(\dot{h}_i - C_p\dot{m}_i T_i) + V_i\frac{dP}{dt}\right]. \tag{2.11}$$

These equations for each of the 11 variables are summarized in Table 2.1. The time evolution of these solution variables can be computed by solving the corresponding differential equations together with appropriate initial conditions.

There are, however, many possible differential equation formulations. Indeed, there are 330 different ways to select four variables from eleven. Many of these systems are incomplete due to the relationships that exist between the variables

Solution variable	Differential equations
i^{th} layer mass	$\frac{dm_i}{dt} = \dot{m}_i$
Pressure	$\frac{dP}{dt} = \frac{\gamma-1}{V}(\dot{h}_L + \dot{h}_U)$
i^{th} layer energy	$\frac{dE_i}{dt} = \frac{1}{\gamma}(\dot{h}_i + V_i\frac{dP}{dt})$
i^{th} layer volume	$\frac{dV_i}{dt} = \frac{1}{\gamma P}\left[(\gamma-1)\dot{h}_i - V_i\frac{dP}{dt}\right]$
i^{th} layer density	$\frac{d\rho_i}{dt} = -\frac{1}{C_pT_iV_i}\left[(\dot{h}_i - C_p\dot{m}_iT_i) - \frac{V_i}{\gamma-1}\frac{dP}{dt}\right]$
i^{th} layer temperature	$\frac{dT_i}{dt} = \frac{1}{C_p\rho_iV_i}\left[(\dot{h}_i - C_p\dot{m}_iT_i) + V_i\frac{dP}{dt}\right]$

Table 2.1: Conservative zone model equations

given in equations (2.7) to (2.11). For example the variables ρ_U, V_U, m_U, and P form a dependent set since $\rho_U = m_U/V_U$ (Jones et al., 2005).

Solution Variables: Four basic variables, the pressure of the compartment P, the volume of the upper layer V_U, the upper and lower layers temperatures, T_U and T_L, have been chosen to describe the condition inside the compartment with the corresponding ordinary differential equations (ODEs) as follows:

$$\frac{dP}{dt} = \frac{\gamma-1}{V}(\dot{h}_L + \dot{h}_U), \tag{2.12}$$

$$\frac{dV_U}{dt} = \frac{1}{\gamma P}\left[(\gamma-1)\dot{h}_U - V_U\frac{dP}{dt}\right], \tag{2.13}$$

$$\frac{dT_U}{dt} = \frac{1}{C_p \rho_U V_U} \left[(\dot{h}_U - C_p \dot{m}_U T_U) + V_U \frac{dP}{dt} \right], \tag{2.14}$$

$$\frac{dT_L}{dt} = \frac{1}{C_p \rho_L V_L} \left[(\dot{h}_L - C_p \dot{m}_L T_L) + V_L \frac{dP}{dt} \right]. \tag{2.15}$$

In these equations, the pressure is taken as the pressure difference relative to an ambient reference pressure to minimize numerical instability (Jones et. al., 2005).

2.2 Governing Equations for Network Modeling

When using a network model to predict smoke movement, the space concerned is regarded as node points. This model is based on the assumption that mixing is complete and the properties of the gas are uniform throughout the node. Due to the above assumption, it is valid only for the compartments remote from the compartment of fire origin. It is much simpler than a zone model. This simplicity makes it useful for the prediction of smoke spreading in high-rise buildings. It is practical and economical to implement the network model for remote rooms in a complex high-rise building fire. The governing equations and source terms for the network model are quite similar to those of the zone model (Yao, et. al., 1999).

Mass Balance: Analyzing smoke movement in a network model in order to establish the mass balance equation of the compartment, we take the mass production rate of a compartment to be equal to the sum of mass flow rate through all the openings of that compartment. The following equation can be established (Liu, et. al., 2001):

$$V_i \frac{\partial \rho_i}{\partial t} + \sum_j (\dot{m}_{ij} - \dot{m}_{ji}) = M_{sup,i}, \tag{2.16}$$

where

V_i = volume of the node i,

ρ_i = smoke density,

$M_{sup,i}$ = mass source or sink in node i,

$\dot{m}_{i,j}$ = mass flow rate from node i to node j,

$\dot{m}_{j,i}$ = mass flow rate from node j to node i.

The mass flow rate through each of the opening can be either unidirectional or bi-directional, and it depends on the temperature difference, pressure difference and the position of the neutral plane between the two adjacent compartments of the opening:

$$\dot{m}_{ij} = f(P_{ij}, T_i, T_j, B, \alpha),$$

where, α is the flow coefficient; B is the width of the opening(m); P_{ij} is the pressure difference at both sides of the openings of compartment i and compartment j (Pa), and T_i and T_j are the temperature of compartment i and compartment j respectively, in K. The detailed calculation of mass flow rate through an opening between two compartments is shown below.

The density of the gas is

$$\rho = \frac{PM_w}{RT}.$$

The mass conservation equation now becomes

$$\sum_j (\dot{m}_{ij} - \dot{m}_{ji}) + V_i \frac{d}{dt}\left(\frac{P_i M_w}{RT_i}\right) = \dot{M}_{sup,i}, \tag{2.17}$$

$$\Rightarrow \frac{d}{dt}(P_i) = \frac{RT_i}{V_i M_w}\left(\dot{M}_{sup,i} - \sum_j (\dot{m}_{ij} - \dot{m}_{ji})\right) + \frac{P_i}{T_i}\frac{d}{dt}(T_i). \tag{2.18}$$

Energy Balance: To analyze the temperature in a compartment, a heat balance equation is set up with the heat production rate and heat flow rate. Based on the relationship between the heat flow rate and room temperature, the set of heat balance equations can be transformed into a set of equations on the temperature of the compartment. The heat balance equation of a compartment is as follows:

$$E_{Li} + E_{Ri} + \triangle E_{Ai} + E_{Wi} = \dot{Q}_i, \tag{2.19}$$

where

E_{Li} = rate of heat carried out by the fire plume through the opening per unit time (kW),

E_{Ri} = rate of radiative heat loss through the opening per unit time (kW),

E_{Wi} = rate of heat absorbed by the wall surfaces per unit time (kW),

$\triangle E_{Ai}$ = rate of heat absorbed by the indoor gases per unit time (kW),

$\dot{Q}_i$ = energy source or sink term (kW).

E_{Li} and E_{Ri} are the sum of heat loss through all of the openings, which can be expressed in terms of the specific heat capacity of air C_p; the area of the opening $A_{Rij}(m^2)$; the emissivity ε ; and the Stefan-Boltzman constant σ, which is set to be $5.6704 * 10^{-8} W m^{-2} k^{-4}$.

$$E_{Li} = \sum_j E_{Lij} = \sum_j (C_{pi} \dot{m}_{ij} T_i - C_{pj} \dot{m}_{ji} T_j), \tag{2.20}$$

$$E_{Ri} = \sum_j E_{Rij} = \sum_j A_{Rij} \varepsilon \sigma (T_i^4 - T_j^4). \tag{2.21}$$

E_{Wi} is the sum of heat absorbed by all of the wall surfaces which can be expressed in terms of the area of the k^{th} wall surface of compartment i - $A_{Wi(k)}(m^2)$; the surface heat exchange coefficient of the k^{th} wall surface of compartment i - $h_{i(k)}(WM^2K^{-1})$ and the surface temperature of the k^{th} wall surface of compartment i - $T_{Wi(k)}(K)$ as:

$$E_{Wi} = \sum_k E_{Wi(k)} = \sum_k A_{Wi(k)} h_{i(k)} (T_i - T_{Wi(k)}). \tag{2.22}$$

Heat absorbed by indoor gases is expressed in terms of the gas density ρ_i; specific heat capacity C_{pi}; volume V_i and temperature T_i of compartment i as:

$$\triangle E_{Ai} = \rho_i C_{pi} V_i \frac{d}{dt}(T_i). \tag{2.23}$$

Substituting equation (2.23) into the energy equation would give an equation with temperature T_i being the unknown:

$$\begin{aligned} &\sum_j (C_{pi} m_{ij} T_i - C_{pj} m_{ji} T_j) + \sum_j A_{Rij} \varepsilon \sigma (T_i^4 - T_j^4) \\ &+ \sum_j A_{Wi(k)} h_{i(k)} (T_i - T_{Wi(k)}) + \rho_i C_{pi} V_i \frac{d}{dt}(T_i) = \dot{Q}_i, \end{aligned} \tag{2.24}$$

$$\Rightarrow \frac{d}{dt}(T_i) = \{\dot{Q}_i - (\sum_j (C_{pi} m_{ij} T_i - C_{pj} m_{ji} T_j) + \sum_j A_{Rij} \varepsilon \sigma (T_i^4 - T_j^4) + \sum_j A_{Wi(k)} h_{i(k)} (T_i - T_{Wi(k)}))\} \frac{RT_i}{P_i C_{pi} V_i M_w}. \quad (2.25)$$

We have established governing equations for the two-zone and network models. To make the connection between the two models, we take the outputs from a room within the two-zone model, which has connections to rooms within the network model, as inputs/sources for the network model. These outputs from a two-zone room are: upper-layer temperature and mass flow going out of that room into network model rooms. In chapter 3 we discuss the implementation of the hybrid model.

Chapter 3

Implementation of the Hybrid Model

The implementation of the hybrid model assumes that there is coupling between the zone and network models. The solution procedure consists of two parts: 1) simulation of two-zone model, which deals with the room with fire origin and rooms near the fire, 2) simulation of the network model, which includes rooms away from the fire.

- Splitting for network model

  A number of experimental studies on network model shows that convergence speeds for pressure is much faster than for temperature, which makes it difficult to choose the desirable time scale when trying to solve pressure and temperature together. In order to address this issue, pressure and tem-

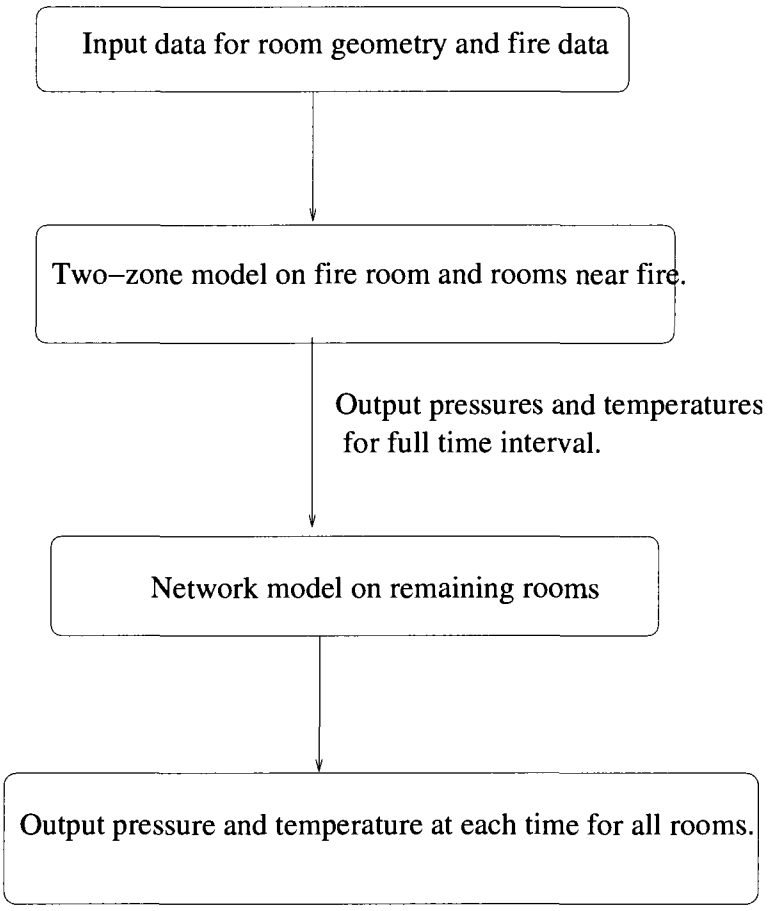

Figure 3.1: Flow chart of the hybrid model

perature may be decoupled so at each time of the simulation the pressure part is solved first, assuming that the temperature remains unchanged. After the pressure solution is obtained, the program then solves the temperature part. Given the different time scales, the error arising from this is negligible and acceptable for the substantial gains in computational efficiency.

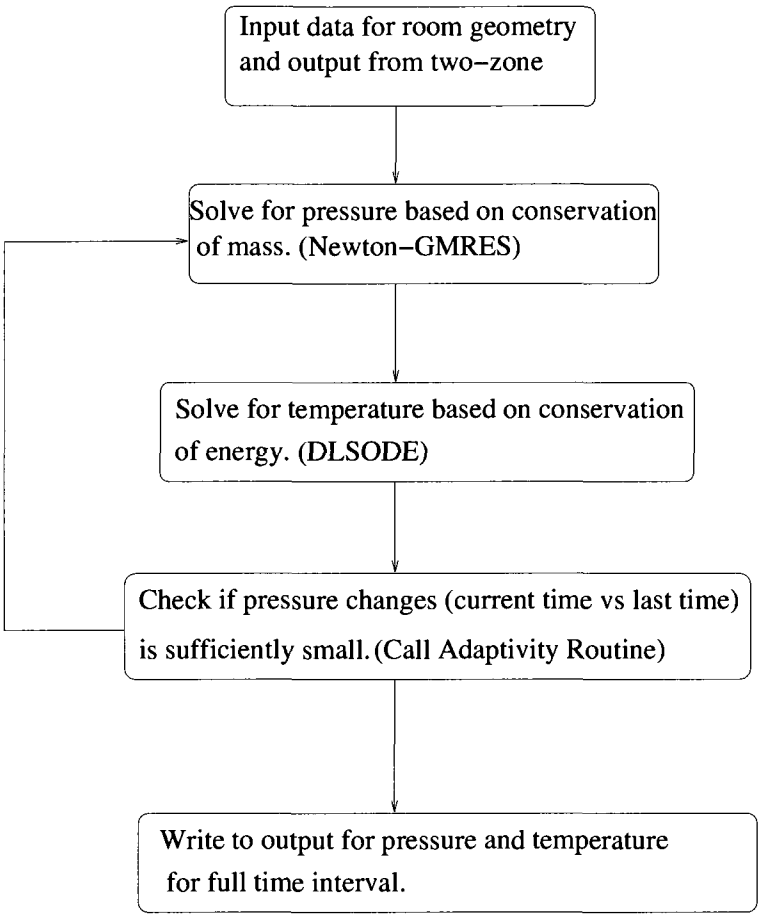

Figure 3.2: Flow chart of Network model

- Adaptive time step

Since the two-zone model consists of a small number of compartments, it is the network model which normally deals with a large number of compartments. As a result, this often causes slow convergence and longer running time. A number of aspects have been considered in order to improve the efficiency of the network model, an important one is the introduction of adaptive time step. Unlike a fixed time step, in which the time step is

given by the user at the beginning of the simulation, an adaptive time step allows the program itself to adjust the time step based on the performance of the solution solve. The basic idea behind the adaptivity algorithms is that, at each time, the program compares the solution of pressure at the current time with previous time's solution. If the change in the solution is greater than a certain tolerance, the time step is then decreased for a more accurate solution. If the change of the solution is smaller than a certain tolerance, then the time step is increased to speed up the simulation time. Therefore by introducing adaptivity, the program should not only perform better for the efficiency of the simulation, but also maintain solution accuracy.

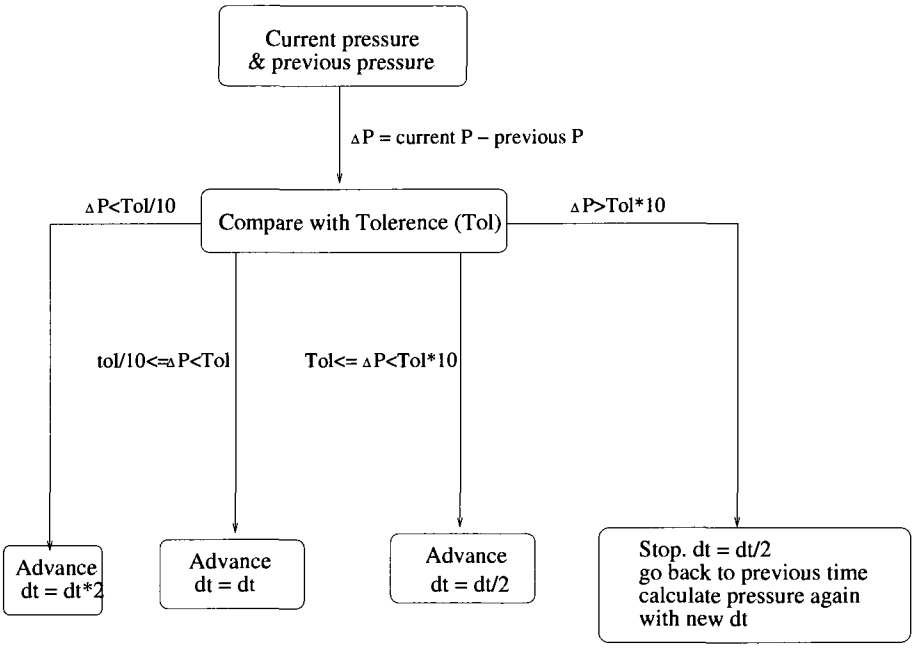

Figure 3.3: Flow chart of adaptivity algorithms

- Newton's method with GMRES

  A Newton-GMRES method is used to solve the system of linear equations for pressures (Equation (2.18)) and find solutions, which are pressures, for each compartment in the building. More discussion of this will be given in the following section.

- DLSODE solver package

  An ODE solver, called DLSODE, is used here to solve the system of non-linear equations for temperatures (Equation (2.25)).

  DLSODE (double precision Livermore Solver for Ordinary Differential Equations) is one of the nine solvers in ODEPACK, which is a collection of Fortran solvers for initial value problem for system of ordinary differential equations.

  DLSODE solves both stiff and nonstiff systems of the form $dy/dt = f(t, y)$. It uses Adams methods in the nonstiff case and Backward Differentiation Formula (BDF) methods in the stiff case. For most cases in our problem, Adams methods for nonstiff systems are applied because of the slow and predictable convergence of temperatures.

- Limitations of implementation

  - Cannot handle isolated rooms in the input building.

    i.e. program will not work if there is a room in the building that has

zero connections to other rooms.

- Needs sufficient connection to ambient for convergence of GMRES.
  For example, each path of mass/energy flow needs to reach the ambient at the end.
- Inner room openings need to be sufficiently large.
  Take the 10-storey tower for example, the area of a vertical opening needs to be larger than .01 m^2.
- Neglects floor thickness in the calculation of vertical flow.
- No feedback between two-zone and network models.

3.1 Numerical Methods for Solving Pressure Equations

As mentioned earlier in this chapter, decoupling pressures and temperatures has been made due to much faster convergence rate for pressures over temperatures. This implies that the most challenging aspect of finding numerical solutions of the model lies in solving the pressure equations (2.18). In this section, we review the main ideas for solving linear and nonlinear equations, and motivate the choices we made.

3.1.1 Methods for Solving Systems of Nonlinear Equations

A system of nonlinear equations is defined as

$$f_n(x) = 0,$$

where n is the dimension of the system, x and $f_n(x)$ are vectors of size n. Finding a solution for a system of nonlinear equations $f_n(x)$ involves finding a solution such that every equation in the nonlinear system is zero. For the case $n = 1$, we simply write $f(x) = 0$.

There are many methods for solving systems of nonlinear equations. We first give a brief discussion of some of the most prevalent methods.

Bisection Methods

One of the simplest methods is called the bisection or interval-halving method of solving the equation $f(x) = 0$. This method is based on the idea that, as long as $f(x)$ is continuous on some interval $[a, b]$, and $f(a)$, $f(b)$ have different signs, there is at least one value of x in the interval $[a, b]$ for which $f(x) = 0$. The bisection method systematically moves the end points of the interval closer and closer together until we obtain an interval of arbitrarily small width that brackets the required root to the desired level of precision. (Mathews and Fink,

1999). For example, given the interval $[a, b]$, and $f(a)$, $f(b)$, the first step of the bisection method evaluates $f(c)$ at $c = (a + b)/2$. Either $f(c) = 0$, in which case we have found a root, or $f(c)$ has the same sign as just one of $f(a)$ or $f(b)$. We then discard the half interval for which there is no sign change, and repeat the bisection method for the remaining interval. There are a few things to note about the bisection method.

1. Many initial inputs are required to start the iteration.
2. If there is more than one root in the interval $[a, b]$, the bisection method will only find one of the roots.
3. Bisection method converges linearly, which is very slow.
4. Not practical for $n \geq 2$.

Fixed Point Methods

Let us begin with the definition of fixed point. A fixed point of a function $g(x)$ is a real number x_p such that $x_p = g(x_p)$.

When attempting to solve the equation $f(x) = 0$ using a fixed point method, the idea behind it is to find a way to re-arrange $f(x) = 0$ in the form:

$$x = g(x).$$

The function g can be defined in many ways. For example, $f(x) = 0$ can be written as $f(x) + x = x$. Then we get $x = g(x)$, where $g(x) = f(x) + x$. Finding a value of x for which $x = g(x)$ is thus equivalent to finding a solution of the equation $f(x) = 0$.

We can say that the function $g(x)$ defines a map, such that for each value of x, the mapping of $g(x)$ gives a new point $\tilde{x}$. Usually this map results in the points x and $\tilde{x}$ being some distance apart. If this is not the case for some $x = x_p$, we say that x_p is a fixed point of $g(x)$. Thus we have $x_p = g(x_p)$, and the fixed point of $g(x)$ is also a root of the corresponding equation $f(x) = 0$.

To find a solution using a fixed point method, we start with an initial value x_0 and then use the iterative rule:

$$x_{k+1} = g(x_k),$$

where $k = 0, 1, 2, \ldots$, and continue iterating until the difference between successive x_k is as small as we require. Then the final value of x_k approximates a fixed point of $g(x)$, and hence approximates a zero of $f(x)$. We now give a convergence theorem for fixed point method.

Theorem - Fixed-Point Theorem (see for example Mathews and Fink, 1999).

Assume that (i) $g, g' \in C[a, b]$, *(ii)* K *is a positive constant, (iii)* $x_0 \in [a, b]$, *and (iv)* $g(x) \in [a, b]$ *for all* $x \in [a, b]$.

If $|g'(x)| \leq K < 1$ *for all* $x \in [a, b]$, *then the iteration* $x_k = g(x_{k-1})$ *will converge to the unique fixed point* $x_p \in [a, b]$. *In this case,* x_p *is said to be an attractive point.*

If $|g'(x)| > 1$ *for all* $x \in [a, b]$, *then the iteration* $x_k = g(x_{k-1})$ *will not converge to* $x_p \in [a, b]$. *In this case,* x_p *is said to be a repelling fixed point and the iteration exhibits local divergence.*

In general, a fixed point method works for multi-dimensional cases, but it is very dependent on the nature of the function g as mentioned in the above theorem. The order of convergence of a fixed point method is p if

$$g'(x) = g''(x) = \ldots = g^{p-1}(x) = 0,$$

$$g^p(x) \neq 0.$$

Newton's Method

Newton's method (also known as the Newton–Raphson method) is perhaps the most useful and best known method for finding successively better approximations to the roots of a real-valued function. In describing Newton's method, consider a function $f(x)$ which has a zero x_p. Given an approximate zero x_0, the next approximation is found by finding the intersection with the x-axis of the tangent at $f(x_0)$. Thus, instead of finding the zero to the function $f(x)$,

Newton's method reduces the problem to finding the root to the linear approximation of $f(x)$ which interpolates $(x_0, f(x_0))$ and has the same slope of $f(x)$ at x_0. Of course, the slope of the curve at $(x_0, f(x_0))$ is given by the derivative at x_0, $f'(x_0)$.

In general, if $f(x), f'(x)$, and $f''(x)$ are continuous near a root x_p, then given an initial approximation x_0 that is near x_p, Newton's method is a good choice to be used to find a root remarkably quickly, and it works for $n \geq 2$. Newton's method gains advantages over methods like bisection because of its faster convergence and lesser requirements for initial inputs. Unlike a fixed point method, whose convergence depends on the nature of the function g, Newton's methods are, in general, applicable to different f. Based on these reasons, we choose Newton's method for solving our problem.

Discussion of Newton's Algorithm

Newton's formula for solving $f(x) = 0$ is:

$$x_{k+1} = x_k - \frac{f(x_k)}{f'(x_k)}, \tag{3.1}$$

where $f'(x_k) \neq 0$. This formula can be derived from Taylor's expansion of $f(x)$ at x_k. Then we have

$$f(x) \approx f(x_k) + f'(x_k)(x - x_k).$$

Then set $f(x) = 0$ to find the next approximation x_{k+1} to the root of $f(x)$,

this gives us equation (3.1), an iteration algorithm which may well converge on to root of $f(x)$, under appropriate conditions.

A few things to note about Newton's algorithm.

1. Newton's method works well in multi-dimensional space, and its dependency on the function f is less restricted than with fixed point and other methods provided the initial guess is close enough.

2. Newton's algorithm requires the evaluation of two functions per iteration, $f(x_k)$ and $f'(x_k)$. In most practical problems, the function may be given by a long and complicated formula, and hence an analytical expression for the derivative may not be easily obtainable. One alternative method, which does not involve evaluations of $f'(x)$ is called the secant method (not discussed in this thesis). It approximates the derivative by using the slope of a line through two points on the function. The secant method has slightly slower convergence to a simple root than Newton's method.

3. If the initial guess is too far from the true root, Newton's method may fail to converge. For this reason, Newton's method is often referred to as a local technique.

4. In order to avoid division-by-zero error, it is clear that $f'(x_k)$ can not equals zero. Similarly, if $f'(x_k)$ is very close to zero, Newton's method may still fail to converge, because the tangent line is nearly horizontal and hence may never pass the desired root.

5. If there are more than one root, there is no general technique for choosing different starting guesses so as to converge to different roots.

6. If a root has higher order multiplicity, the convergence rate of Newton's method may be reduced. Fast convergence may be obtained by a modification of Newton's method.

We had a brief discussion of Newton's method on solving $f(x) = 0$. But how to solve a system of nonlinear equations, i.e., $f_n(x) = 0$, when n gets large, using Newton's method?

As mentioned earlier, Newton's method requires the evaluation of derivative of function f at each iteration. When it comes to solving a higher dimensional system $f_n(x) = 0$, instead of dividing derivatives $f_n^{'}(x_k)$ in the Newton's formula, the generalized formula involves the inverse of the n-by-n Jacobian matrix $J_n(x_k)$ at each iteration. It becomes

$$J_n(x_k)(x_{k+1} - x_k) = -f_n(x_k),$$

where x_k and x_{k+1} are size n vectors in this formula. Rather than actually computing the inverse of this matrix, which would take lots of time and memory space even for present-day computers when n gets big, we can solve this formula as a system of linear equations in the form $Ax = b$, where $(x_{k+1} - x_k) = x$ is the unknown. A method of solving linear equations can then be implemented at each step of Newton's iteration. We will discuss the methods of solving system of linear equations shortly.

Convergence of Newton's Method

Let us begin with a formal Newton's theorem for convergence when $n = 1$.

Newton's Theorem (see for example Mathews and Fink, 1999).

Assume that $f \in C^2[a, b]$ *and there exists a number* $x_p \in [a, b]$, *where* $f(x_p) = 0$. *If* $f'(x_p) \neq 0$, *then there exists a* $\delta > 0$ *such that the sequence* $\{x_k\}_{k=0}^{\infty}$ *defined by the iteration*

$$x_k = g(x_k - 1) = x_{k-1} - \frac{f(x_{k-1})}{f'(x_{k-1})} \quad \textit{for } k = 1, 2, \ldots \tag{3.2}$$

will converge to x_p *for any initial approximation* $x_0 \in [x_p - \delta, x_p + \delta]$.

where the function $g(x)$ defined by formula

$$g(x) = x - \frac{f(x)}{f'(x)},$$

is called the Newton iteration function.

Proving this theorem is to understand why x_0 needs to be close to the root x_p. Again, we start with the Taylor expansion of $f(x)$ at x_0.

$$f(x) = f(x_0) + f'(x_0)(x - x_0) + \frac{f''(x_0)}{2!}(x - x_0)^2 + \ldots,$$

substituting $x = x_p$ into the equation and using the fact that $f(x_p) = 0$ gives

$$0 = f(x_0) + f'(x_0)(x_p - x_0) + \frac{f''(x_0)}{2!}(x_p - x_0)^2 + \ldots.$$

If x_0 is close enough to x_p, then the terms beyond first order in the equation above will be small compared to the sum of the first two terms. Hence we have the approximation

$$0 \approx f(x_0) + f'(x_0)(x_p - x_0),$$

$$\Rightarrow$$

$$x_p \approx x_0 - \frac{f(x_0)}{f'(x_0)}.$$

This is an iteration starting from the approximation x_1 to the root

$$x_1 \approx x_0 - \frac{f(x_0)}{f'(x_0)}.$$

Equation (3.2) is established when x_0 is replaced by x_{k-1} in the above equation. Next we give a theorem for the performance of Newton's method.

Theorem - Convergence rate for Newton's method (see for example Mathews and Fink, 1999).

Assume that Newton's iteration produces a sequence $\{x_k\}_{k=0}^{\infty}$ *that converges to the root* x_p *of the function* $f(x)$. *If* x_p *is a simple root, convergence is quadratic and*

$$|E_{k+1}| \approx \frac{|f''(x_p)|}{2|f'(x_p)|}|E_k|^2 \quad \textit{for } k \textit{ sufficiently large.}$$

If x_p *is a multiple root of order* M, *convergence is linear and*

$$|E_{k+1}| \approx \frac{M-1}{M}|E_k| \quad \textit{for } k \textit{ sufficiently large.}$$

In the above theorem, we define: $E_k = x_p - x_k$, and $E_{k+1} = x_p - x_{k+1}$.

3.1.2 Methods for Solving Systems of Linear Equations

A system of linear equations can be written in the matrix notation as

$$Ax = b. \tag{3.3}$$

There are two basic classes of methods for solving system (3.3). The first class is represented by direct methods. They theoretically give an exact solution in a (predictable) finite number of steps. Most popular direct methods are Gaussian Elimination; Orthogonalization and Householder Transformations. The second class is called iterative methods (originally developed by Gauss in 1823, Liouville in 1837, and Jacobi in 1845), which construct a series of solution approximations that (under some assumptions) converge to the solution of the system.

One of the simplest direct method to solve linear systems of equations (3.3) is Gaussian elimination, it transforms a full linear system into an upper-triangular one by applying simple linear transformations on the left. (Trefethen and Bau, 1997). For an n-by-n matrix A, Gaussian elimination transforms A into an n-by-n upper-triangular matrix by introducing zeros below the diagonal. However, Gaussian elimination is unstable for solving general linear systems for the follow-

ing reasons: 1). If some pivot in A is equals 0, then the elimination fails because of the divided-by-zero situation; 2). If the value of some pivot in A is very small compared to other numbers in A, then the computation may be numerically unstable. To address the instability issue with Gaussian elimination, pivoting was introduced and has been a standard feature of Gaussian elimination computations since the 1950s. In general, by interchanging rows and perhaps columns of matrix A, Gaussian elimination with pivoting can significantly improve stability over Gaussian elimination without pivoting. There are two methods of pivoting: complete pivoting and partial pivoting. In practice. complete pivoting is not recommended since it normally costs $O(m^3)$ operations to the Gaussian elimination. On the other hand, partial pivoting is considered to be equally good and cost $O(m^2)$ overall. For detailed reviews on Gaussian elimination and pivoting, see (Trefethen and Bau, 1997).

Direct methods vs. Iterative methods

Direct methods work well for systems with matrix A of modest size, but not necessarily optimal for an arbitrary system (3.3). Many applications require the solution of very large systems of linear equations $Ax = b$ in which the matrix A is sparse, i.e., has only relatively few nonzero elements. The classical elimination methods are not suitable in this context since they tend to lead to the formation of dense intermediate matrices, making the number of arithmetic operations necessary for the solution too large even for present-day computers, not to mention the fact that the memory requirements for such intermediate

matrices exceed available space (Stoer, 2002). In general, direct methods for a matrix with of size n require $O(n^3)$ operations, which can be very prohibitive when n gets large.

For these reasons, researchers have moved to iterative methods for solving such systems of equations. Embodying an approach quite different from that behind direct methods such as Gaussian elimination, these methods start with an initial vector x_0 and subsequently generate a sequence of vectors

$$x_0 \rightarrow x_1 \rightarrow x_2 \rightarrow \ldots,$$

which converge toward the desired solution x. An advantage of iterative methods is that one can carry out a relatively large number of iterations with a reasonable amount of effort, since the effort required for an individual iteration step $x_i \rightarrow x_{i+1}$ is essentially equal to that of multiplying a vector by the matrix A (provided A is sparse unstructured). Furthermore, the sparsity of the matrix A can be fully exploited, and computer storage is required only for the nonzero entries of A and vector x, plus one or two more vectors. Compared to direct methods, iterative methods require $O(n^2)$ or less operations depending on the sparsity of the matrix, and the number of iterations required.

Krylov Subspace Methods

Many important iterative techniques available for solving large linear systems are based on the idea of projecting an N-dimensional problem into a lower-

dimensional Krylov subspace. Given a matrix A and a vector b, the associated Krylov sequence is spanned by the set of vectors b, Ab, A^2b, A^3b, ..., and the corresponding Krylov subspaces are the spaces spanned by successively larger groups of these vectors.(Trefethen and Bau, 1997).

Overview of Krylov subspace

Two best known variants of Krylov subspace methods are: the classical conjugate-gradient method and GMRES method, which stands for "generalized minimal residuals". The conjugate gradient method is the "original" Krylov subspace method. Discovered by Hestenes and Stiefel in 1952, it solves symmetric positive definite systems of equations amazingly quickly if the eigenvalues are well distributed (Trefethen and Bau, 1997). On the other hand, the GMRES method, developed by Saad and Scheltz in 1986, is more expensive but is applicable to more general linear systems with a non-symmetric nonsingular matrix A.

Back to our problem. First we define the adjacency matrix as: the ijth and jith entries of the adjacency matrix are non-zero only if there is a connection between two compartments i and j, and a compartment is always self-connected (i.e. entries in the main diagonal are non-zero). We know that this adjacency matrix in the system is sparse, based on the fact that the number of connections to a compartment is generally much less than the total number of compartments. Furthermore, the matrix associated with the system is, in general, not necessarily

positive definite and symmetric. In order to make our smoke model suitable for different building configurations, the GMRES method is our choice. Next, we will discuss this method in more details.

Arnoldi Iteration

For solving system (3.3), similar to Gram-Schmidt orthogonalization, which orthogonalizes A by a succession of triangular operations. Arnoldi iteration is an algorithm for building an orthogonal basis of the Krylov subspace, and computes a Hessenberg reduction $A = QHQ^T$, where Q is an orthogonal matrix and H is in Hessenberg form.

Let $Q_n = [q_1, q_2, \ldots, q_n]$ and $\mathcal{K}_n$ be the Krylov subspace $[b, Ab, \ldots, A^{n-1}b]$. Starting with q_1 as any unit vector, the Arnoldi procedure successively finds orthonormal vectors q_2, q_3, ..., q_{n+1} which form a basis for $\mathcal{K}_n$. This procedure also produces an $(n+1)$-by-n upper Hessenberg matrix $\tilde{H}_n$ with

$$AQ_n = Q_{n+1}\tilde{H}_n.$$

GMRES Method

Let x_* be the exact solution of system (3.3). The idea of GMRES is that, at step n, we shall approximate x_* by the vector $x_n \in \mathcal{K}_n$ that minimizes the norm of the residual $r_n = b - Ax_n$ (Trefethen and Bau, 1997).

With Q_n and $\tilde{H}_n$ given by Arnoldi iteration, the vector $x_n \in \mathcal{K}_n$ can be written as $x_n = Q_n y$ with $y \in \mathcal{R}^n$. Then

$$|r_n| = |AQ_n y - b|,$$

$\Rightarrow$

$$|r_n| = |Q_{n+1}\tilde{H}_n y - b|.$$

The $|.|$ used here refers to the standard 2-norm. Because Q is orthonormal, we have

$$|r_n| = |\tilde{H}_n y - b|,$$

where $b = (|b|, 0, 0, \ldots, 0)$ is an $(n+1)$ vector.

Hence, x_n can be found by minimizing the norm of the residual r_n. Now the problem becomes a linear least squares problem of size n.

Part of the GMRES method is to find the vector y which minimizes

$$|\tilde{H}_n y - b|.$$

This can be done by computing a QR factorization of $\tilde{H}_n$ such that

$$\tilde{H}_n = \tilde{Q}_n \tilde{R}_n,$$

where $\tilde{Q}_n$ is an $(n+1)$-by-n matrix, and its inner n-by-n matrix is orthogonal. $\tilde{R}_n$ is an n-by-n upper triangular matrix.

Let $\tilde{H}_n y = \tilde{Q}_n c$, where $c = \tilde{R}_n y$. Now we want to minimize $|r_n| = |\tilde{Q}_n c - b|$. This gives

$$c = \tilde{Q}_n^T b.$$

Then solving $\tilde{R}_n y = c$ will give the optimal y for $|A\tilde{Q}_n y - b|$.

Convergence of GMRES

The convergence of GMRES, in general, depends on the conditioning of matrix A and the existence of polynomials which are small on the spectrum of A. Let us begin by stating a global convergence result.

Theorem (Saad, 1996)

If A is a positive definite matrix, then GMRES(n) converges for any $n \geq 1$.

The n in the above theorem denote the dimension of the Krylov subspace. This theorem, however, is not necessarily applicable to our problem, since the eigenvalues of matrix A in our system are not always positive, which means A is not always positive definite. Next we like to establish a result which would provide an upper bound on the convergence rate of GMRES.

At step n, we define the residual

$$r_n = b - Ax_n.$$

At step $n+1$, we define the residual

$$r_{n+1} = b - Ax_{n+1}.$$

First note that the norm of residual $r_{n+1} \leq$ the norm of residual r_n, because x_{n+1} is minimized over $\mathcal{K}_{n+1}$, and we know that $\mathcal{K}_{n+1} \supseteq \mathcal{K}_n$, where $\mathcal{K}_n$ is the space over which x_n is minimized. Moreover, it is clear that $r_N = 0$, since we now minimize over the entire space which will give the exact solution $x_N = x_*$. However, we like to find an optimal $n << N$, such that r_n is minimized over $\mathcal{K}_n$.

Earlier, we define Krylov subspace $\mathcal{K}_n = \text{span}\,[b, Ab, , \ldots, A^{n-1}b]$. This gives

$$x_n = c_1 b + c_2 Ab + , \ldots, + c_n A^{n-1} b =: q_n(A)b,$$

for some constants c_i, and q_n is an $n-1$ degree polynomial. Then the residual at step n becomes

$$r_n = b - Ax_n = b - Aq_n(A)b = p_n(A)b,$$

where p_n is an n^{th} degree polynomial.

The Schwarz inequality gives us

$$|r_n| = |p_n(A)b| \leq |p_n(A)||b|,$$

$\Rightarrow$

$$\frac{|r_n|}{|b|} \leq |p_n(A)|.$$

With this given upper bound, we need to find out how small can $|p_n(A)|$ be? This will, in general, depend on the structure of matrix A. Suppose A is diagonalizable such that $A = X\Lambda X^{-1}$, where Λ is the diagonal matrix of eigenvalues. Then

$$|p_n(A)| \leq |X||p_n(\Lambda)||X^{-1}| = k(X) \max_{i \in 1:N} p_n(\lambda_i),$$

where $k(X) = |X||X|^{-1}$ is the condition number of X. The residual at step n is then bounded by

$$|r_n| \leq k(X) \max_{i \in 1:N} p_n(\lambda_i). \tag{3.4}$$

The above inequality tells us that the residual r_n is affected by both $k(X)$ and $\max_{i \in 1:N} p_n(\lambda_i)$. Given the n^{th}-degree polynomial p_n, $\max_{i \in 1:N} p_n(\lambda_i)$ gives the largest value of p_n for any λ_i. In other words, if the eigenvalues of matrix A are closed together on the axis, then the condition number $k(A)$ is small, and $\max_{i \in 1:N} p_n(\lambda_i)$ is small as well. However, if the eigenvalues of A are 'spread out' on the axis, then we have a large $k(A)$, and $\max_{i \in 1:N} p_n(\lambda_i)$ is also large. In summary, fast convergence occurs when both $k(X)$ and $k(A)$ are small.

Discussion of Condition Numbers

We will pick three examples from chapter 4 and discuss the condition numbers of the adjacency matrix A and eigenvector matrix X. Note that all three examples are isothermal simulations such that a constant mass source is put into one compartment of the building throughout the simulation. For all of our examples,

	4-room case	12-room case	61-room case
$k(A)$ at early stage	9	23000	909070
$k(A)$ at last time	9	12508	121190

Table 3.1: Condition number of A - $k(A)$

$k(X)$ is close to 1 at both early stage and the last time step. Hence the residual r_n is determined by $\max_{i \in 1:N} p_n(\lambda_i)$, which is related to $k(A)$ in Table 3.1. Table 3.1 lists $k(A)$ at both the early stage and the last time step of the simulation.

The geometries and the tables of mass flow rate for these examples are illustrated in chapter 4. Let us first look at a simple 4-room building case for network model. The geometry of this building (see Figure 4.2) shows that all compartments are well connected, both with each other and to ambient. This suggests that the mass source is distributed from compartment-1 to the other compartments very quickly. As a result, the condition number of A remains unchanged during the simulation. Table 4.5 shows that the mass entering into compartment-1 is evenly distributed to all other compartments. This indicates matrix A is well-conditioned.

Next we move on to a 12-room building case. Figure 4.6 shows the geometry of this building. First notice that the condition number of matrix A is big, indicating that a lot is happening on part of A while other parts remain settled. This can be explained by looking at Table 4.10. A big portion of the mass,

coming out of compartment-11, is going into a compartment on the first floor. However, only a small amount of the mass is moving upward to the second and third floor. Because of the simple connectivity of this building, the condition number changes only slightly during the simulation.

The last case is a 61-room building example, see Figure 4.8 for the geometry of this building. A larger condition number is expected based on the geometry of this building and the size of the associated matrix A. Table 3.1 shows a big change of the condition number through the simulation. The reason is that rooms, like compartment-60, need much longer time to receive mass flow from compartment-61, comparing to other rooms that are adjacent to compartment-61. As a result, we get a very large condition number at the early stage of the simulation, but once the system reaches equilibrium, the condition number comes down.

Chapter 4

Experimental Results and Discussion

This chapter provides a detailed description of the test results, including a description of each case studied, geometry of the building, output from the simulation and visualization of the output.

4.1 Small Building Simulations

We start with small building simulations for two-zone and network models since they are simple and easy to implement.

4.1.1 Comparison between Two-Zone Model and CFAST

- Geometry of the building

  A simple two-storey four-compartment building is designed here for the simulation using the two-zone model. The fire is located in compartment-1, three windows/doors connect compartments 1, 2, 3 and ambient, two ceiling vents connect compartments 3, 4 and ambient. Figure 4.1 shows the geometry of the building, Table 4.1 shows the dimensions of the four compartments.

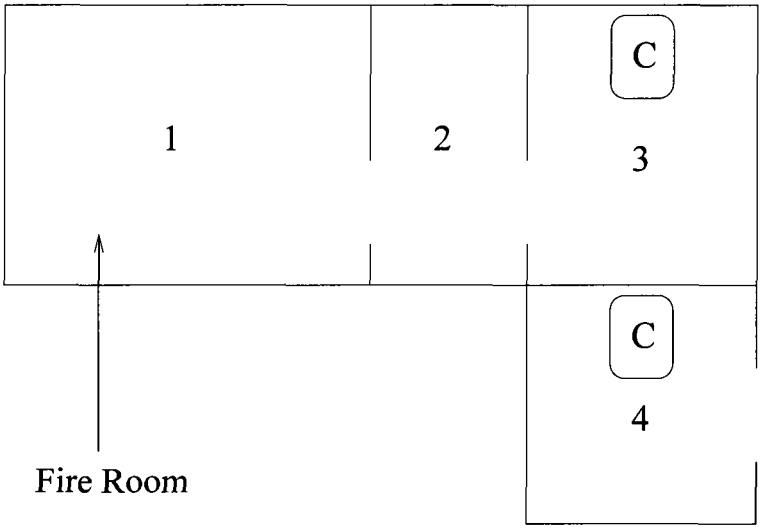

1st floor: Compartment 4.
2nd floor: Compartments 1, 2, 3
C: Ceiling vent.

Figure 4.1: Geometry of 2-storey 4-room building for 2-zone model

	Width(m)	Depth(m)	Ceiling Height(m)	Floor Elevation(m)
1	7.78	8.9	3.3	3.3
2	2.3	1.09	3.3	3.3
3	5	2.46	3.3	3.3
4	5	2.46	3.3	0

Table 4.1: Compartment dimension of the 4-room 2-storey building for 2-zone model.

- Simulation

  The purpose of this simulation is to compare the two zone model with CFAST. The size of the fire for the two zone model, with maximum heat release rate equals to 1 MW, is calculated using the quadratic equation:

  $$HRR = \alpha t^2,$$

  where HRR is the heat release rate, α is a constant (in this case $\alpha = 42.19$), t is time in seconds.

  Table 4.2 shows the temperature comparison for the two models at the last time step. It indicates that the two models have the same pattern of temperature changes, i.e., temperature in fire room rises the quickest, while temperature in room 4 at the lower floor remains unchanged because hot air only goes up. We need to mention that, due to their difference in conduction and radiation rates, defining and predicting exactly the same fires for the two models are not trivial. As a result of that, we see temperature discrepancies shown in the table.

Compartment	Temperature(°C) - 2-zone	Temperature(°C) - CFAST
1	258	299
2	179	208
3	92	91
4	20	20

Table 4.2: Temperature comparison between 2-zone model and CFAST.

	Width(m)	Depth(m)	Ceiling(m)	Floor(m)	Initial Temperature(K)
1	6	5	3	0	350
2	6	5	3	0	280
3	6	5	3	3	293
4	6	5	3	3	300

Table 4.3: Compartment dimension and initial states for the 4-room 2-storey building - Network model.

4.1.2 Network Model

1. Two-storey four-room building

   - Geometry of the building

     This building consists of two floors, each floor has two compartments. Four vertical vents (doors/windows) are included in the building, plus one ceiling vent connect compartments 1 and 3. Figure 4.2 shows the geometry of this building.

   - Simulation

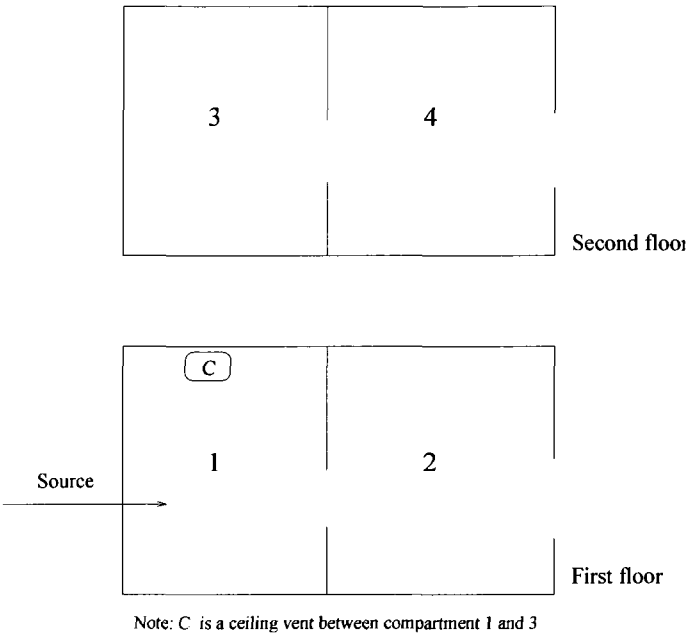

Figure 4.2: Geometry of 2-storey 4-room building - Network model

This building is designed for testing the following cases:

(a) Using initial temperatures in Table 4.3 without any mass source

Four compartments in this building start with various initial temperatures, Figure 4.3 shows that, With a higher initial temperature in compartment-1, the hot air inside the room is pushed into the other compartments through doors/windows and ceiling vent. It forces temperatures in the other three rooms to go up at the early stage of the simulation. Then with the connection made between compartments and ambient, temperatures gradually approach $293K$ (ambient temperature).

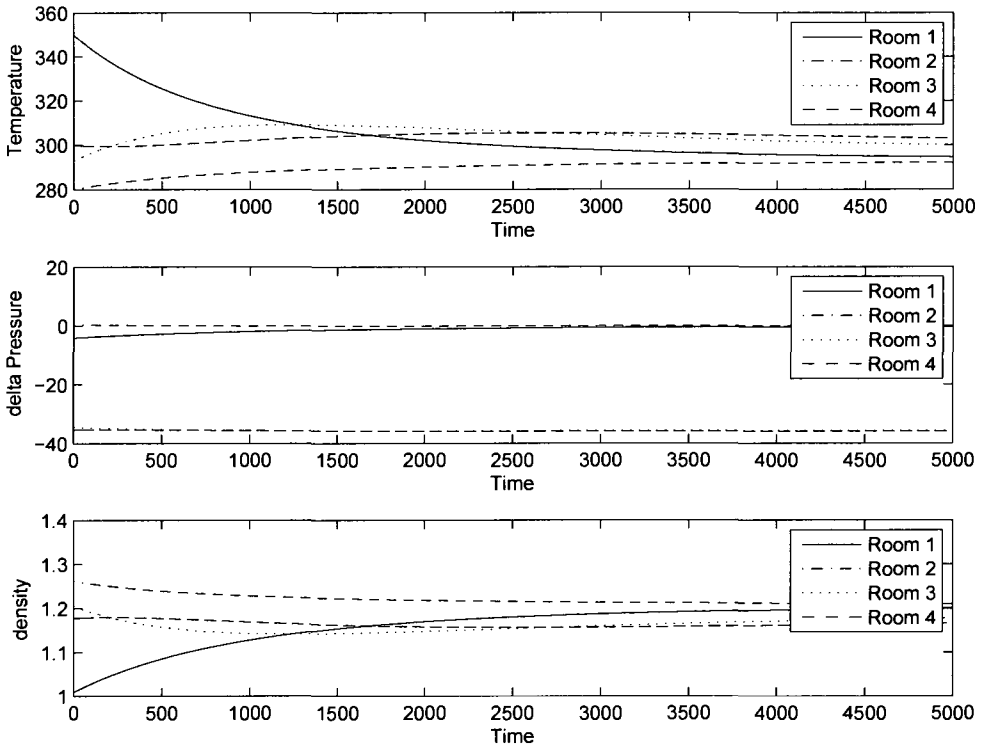

Figure 4.3: Plot of 2-storey 4-room building with no source - Network model. (Temperature in K, Pressure in Pa, Density in Kg/m^3, Time in s)

Table 4.4 lists mass exchanges through each opening in the building. Since there is no mass source introduced into the building, only a small amount of mass exchange caused by temperature difference happens during the simulation. The last-time-step temperatures for each compartment are shown in Table 4.6.

From(room)	To(room)	Mass flow rate(kg/s) -Network
2	1	$6.74 * 10^{-2}$
Ambient	2	$6.73 * 10^{-2}$
3	4	$6.67 * 10^{-2}$
4	Ambient	$7.17 * 10^{-2}$
(Ceiling) 1	3	$6.72 * 10^{-2}$

Table 4.4: Mass flow rate for 4-room 2-storey building - Network model with no source.

(b) Isothermal case with ambient initial states

In this case, all four compartments in the building start with ambient pressure and temperature, a constant mass source (1.5 Kg/s) with ambient temperature is placed into compartment-1. Figure 4.4 shows that temperatures in all four compartments stay unchanged, since there is no energy exchange during the simulation. Pressure in each compartment changes once at the beginning of the simulation based on the amount of mass each compartment obtains. Table 4.5 shows that, the amount of mass entering into compartment-1 merges into ambient through two paths: 1) compartment-1 $\rightarrow$ compartment-2 $\rightarrow$ ambient; 2) compartment-1 $\rightarrow$ compartment-3 $\rightarrow$ compartment-4 $\rightarrow$ ambient.

Table 4.6 lists last time step temperature for each compartment in the building.

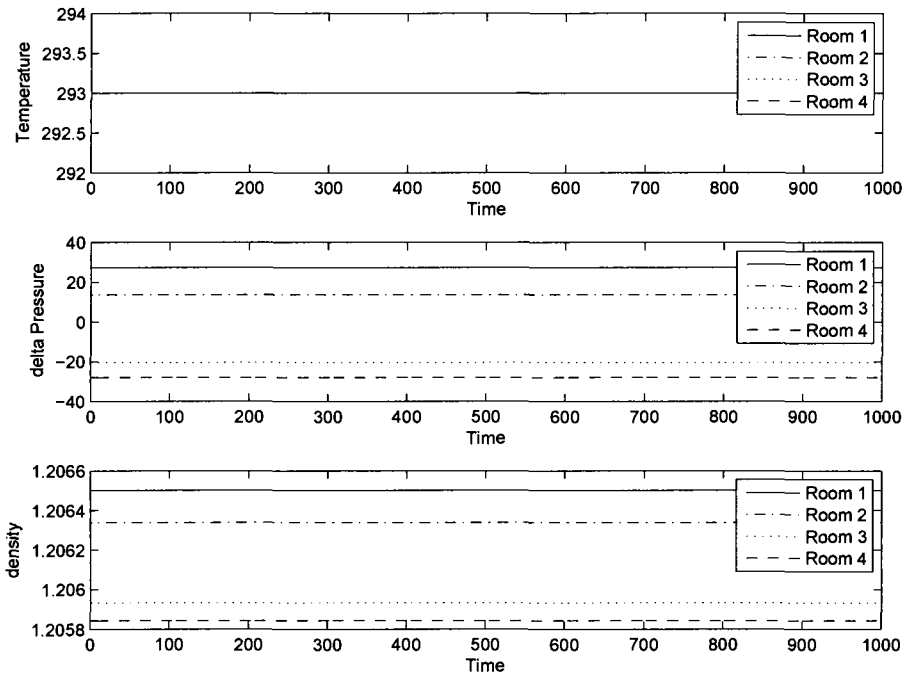

Figure 4.4: Plot of 2-storey 4-room building: isothermal case - Network model. (Temperature in K, Pressure in Pa, Density in Kg/m^3, Time in s)

(c) Non-isothermal case with ambient initial states

In this case, all four compartments in the building start with ambient pressure and temperature, a constant mass source (1.5 Kg/s) with high temperature ($350K$) is placed into compartment-1. As shown in Figure 4.5, temperature in compartment-1 rises first and gets to $350K$ in the shortest time. While compartment-4 is far away from the source compared to the other compartments, temperature inside the room starts to rise the last and takes longer time to reach $350K$. Similar to the isothermal case, Table 4.5 shows two paths of mass exchange for non-isothermal

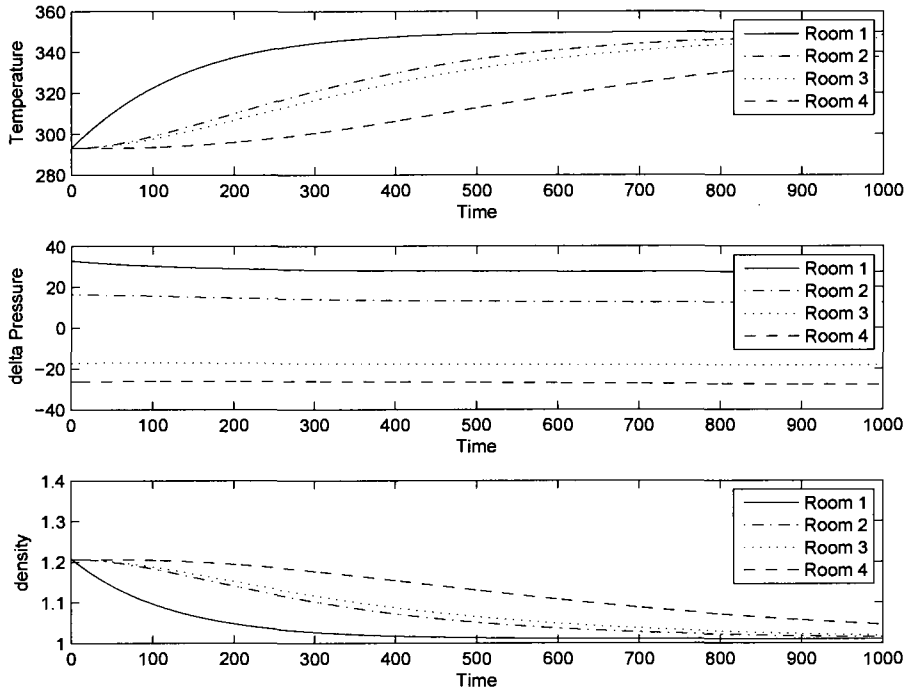

Figure 4.5: Plot of 2-storey 4-room building: non-isothermal case - Network model. (Temperature in K, Pressure in Pa, Density in Kg/m^3, Time in s)

case, with the addition of mass exchange caused by temperature difference.

Table 4.6 lists the last-time-step temperature for each compartment in the building.

From(room)	To(room)	Mass flow rate(kg/s) -Isothermal case	Mass flow rate(kg/s) -Non-isothermal case
1	2	0.756	0.713
2	Ambient	0.756	0.716
3	4	0.744	0.789
4	Ambient	0.744	0.796
(Ceiling) 1	3	0.744	0.787

Table 4.5: Mass flow rate for 4-room 2-storey building - Network model.

Room	Temperature(K) -With no mass source	Temperature(K) -Isothermal case	Temperature(K) -Non-isothermal case
1	293.9	293	350
2	292.3	293	347.4
3	298.6	293	348
4	302.2	293	341.7

Table 4.6: Temperatures for 4-room 2-storey building - Network model.

	Width(m)	Depth(m)	Ceiling Height(m)	Floor Elevation(m)
1	6	5	3	6
2	6	5	3	6
3	12	5	3	6
4	12	3	3	6
5	6	5	3	3
6	6	5	3	3
7	12	5	3	3
8	12	3	3	3
9	6	5	3	0
10	6	5	3	0
11	12	5	3	0
12	12	3	3	0

Table 4.7: Compartment dimension of the 12-room 3-storey building.

2. Three-storey 12-room building

   - Geometry of the building

     This building consists of three floors, each floor has four compartments. A total of 22 vents are opened on external and internal walls, two ceiling vents, which are located in compartment 4 and compartment 8, connect all three floors together. Figure 4.6 shows the geometry of the building, and Table 4.7 shows the dimension of each compartment in this building

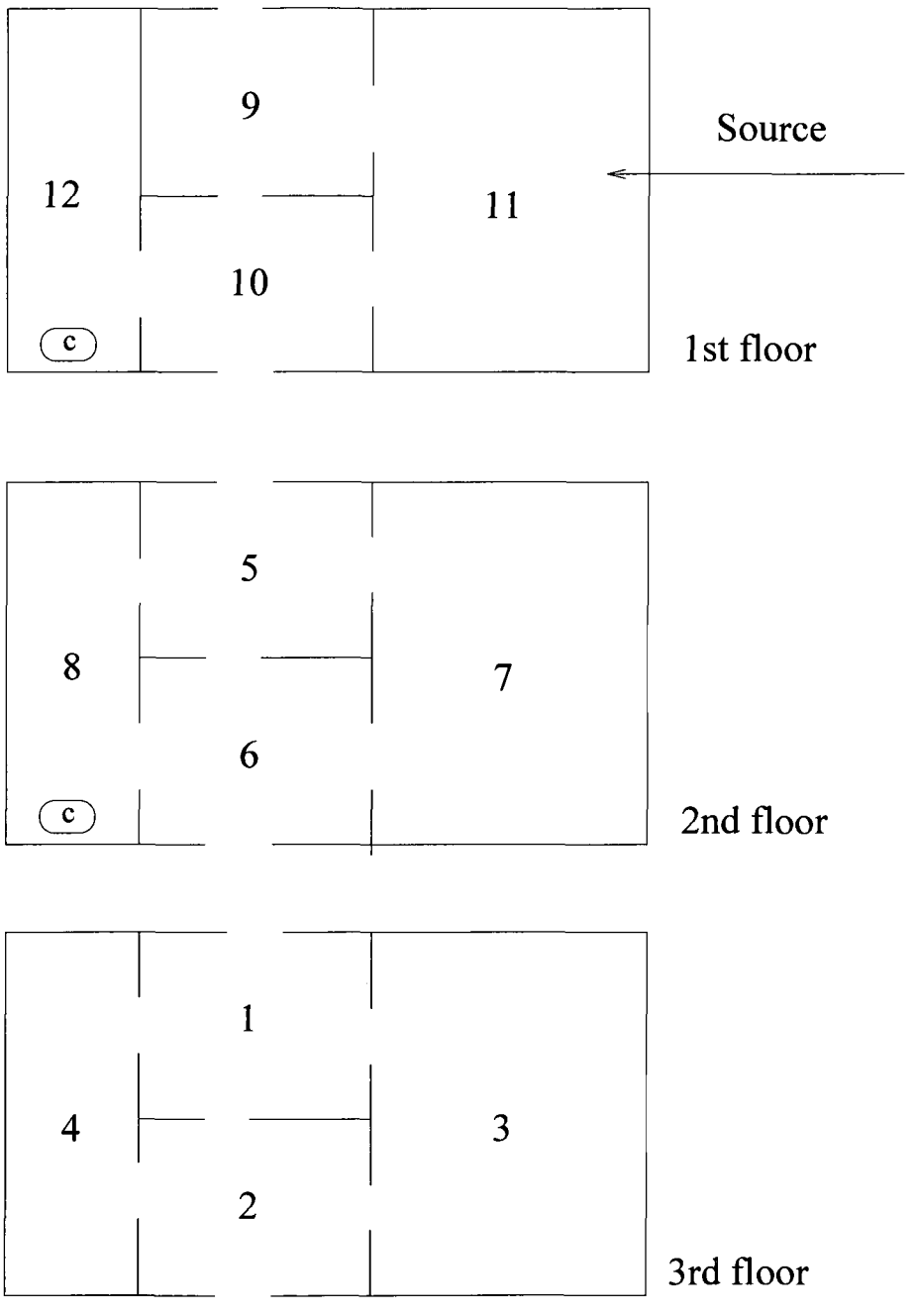

Note: C means ceiling vent.

Figure 4.6: Geometry of 3-storey 12-room building

- Simulation

Both isothermal and non-isothermal cases are simulated in this building, and a comparison between the network model and CONTAM (i.e. mass flow rate) is made for the isothermal case.

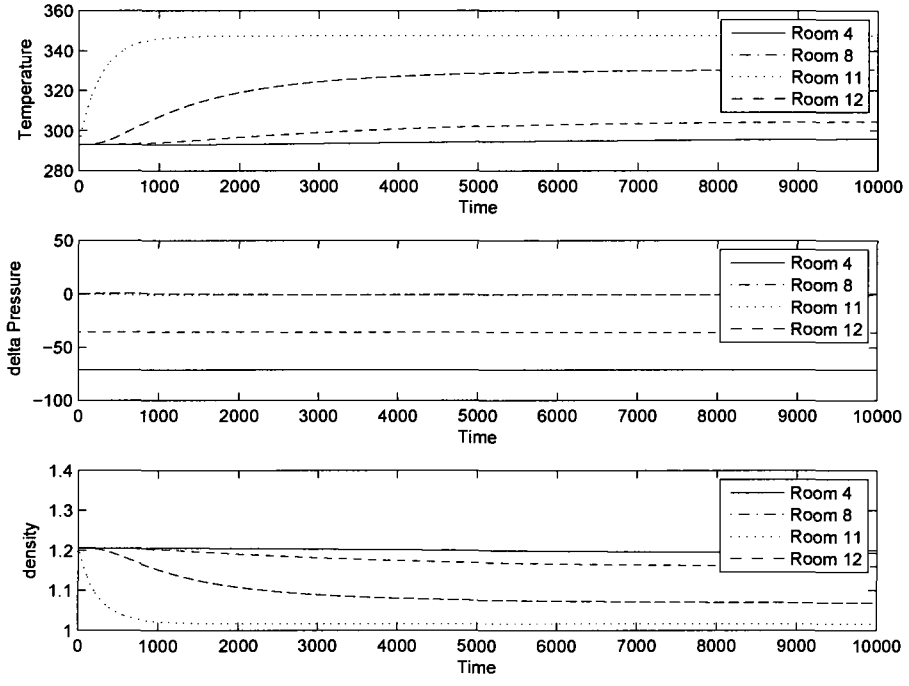

Figure 4.7: Plot for the 3-storey 12-room building - non-isothermal case (Temperature in K, Pressure in Pa, Density in Kg/m^3, Time in s)

For the non-isothermal case, a constant mass source of $1.5Kg/s$ with temperature $350K$ is placed into compartment-11. Four compartments are chosen for visualization of the simulation. Shown in Figure 4.7, temperatures in four compartments approach $350K$ at different speed based on the location of the compartments. Table 4.8 and Table

4.9 list mass flow rates and temperature solutions of this case.

A comparison between the network model and CONTAM is made in order to test the accuracy of results. Both models take a constant mass source of $1.5Kg/s$ with ambient temperature into compartment-11 at the ground floor. Shown in Table 4.10, both models indicate that the majority of the mass entering compartment 11 at first floor goes into ambient through compartments 9 and 10, and the results match quite well for mass flow rates at the first floor. At the second and third floors, we see a difference in mass flow rates between the two models. These small discrepancies are acceptable, and could be caused by rounding errors or the different tolerance used in the programs.

Room ♯1	Room ♯2	Mass flow rate(kg/s) -from ♯1 to ♯2	Mass flow rate(kg/s) -from ♯2 to ♯1
1	2	$6.07 * 10^{-3}$	$6.18 * 10^{-3}$
1	3	$9.26 * 10^{-2}$	0.11
1	4	0.12	0.15
2	4	0.12	0.15
2	3	$9.24 * 10^{-2}$	0.11
5	6	$6.8 * 10^{-3}$	$6.73 * 10^{-3}$
5	7	0.16	0.19
5	8	0.24	0.26
6	8	0.24	0.26
6	7	0.16	0.19
9	Ambient	1.08	0.37
9	10	$4.05 * 10^{-2}$	0
9	11	$9.39 * 10^{-2}$	0.84
10	Ambient	1.08	0.37
10	12	$8.31 * 10^{-2}$	0
10	11	$9.35 * 10^{-2}$	0.84
1	Ambient	$7.6 * 10^{-2}$	$3.96 * 10^{-2}$
2	Ambient	$7.59 * 10^{-2}$	$3.96 * 10^{-2}$
3	Ambient	$3.07 * 10^{-2}$	$5.99 * 10^{-2}$
5	Ambient	0.14	$9.37 * 10^{-2}$
6	Ambient	0.14	$9.37 * 10^{-2}$
7	Ambient	$7.37 * 10^{-2}$	0.12
(Ceiling) 4	8	0	$4.31 * 10^{-2}$
(Ceiling) 8	12	0	$8.31 * 10^{-2}$

Table 4.8: Mass flow rate for 12-room 3-storey building - non-isothermal case.

Room	Temperature(K)	Room	Temperature(K)
1	294.7	7	298.1
2	294.7	8	304.5
3	294	9	330.8
4	295.9	10	330.8
5	300.2	11	347.5
6	300.2	12	330.5

Table 4.9: Temperatures for 12-room 3-storey building - non-isothermal case.

4.2 Large Building Simulations of Network Model

One-storey 61-compartment building

- Geometry of the building

  This one-storey building consists of 61 rooms, for simplicity all compartments have the same dimension, a total number of 100 doors/windows are opened to external and internal walls, again for simplicity all openings have the same size ($0.25m^2$). Table 4.11 shows the dimensions of the compartments in the building. Figure 4.8 shows the layout of the building and the location of the openings.

- Simulation

From(room)	To(room)	Mass flow rate-CONTAM	Mass flow rate-Network
1	2	0	$4.2 * 10^{-4}$
1	3	$1.98 * 10^{-5}$	$6.5 * 10^{-4}$
2	3	$1.96 * 10^{-5}$	$9.08 * 10^{-4}$
3	Ambient	$3.96 * 10^{-5}$	$1.61 * 10^{-3}$
4	1	$7.92 * 10^{-5}$	$2.55 * 10^{-3}$
4	2	$7.92 * 10^{-5}$	$2.55 * 10^{-3}$
1	Ambient	$5.94 * 10^{-5}$	$1.71 * 10^{-3}$
2	Ambient	$5.94 * 10^{-5}$	$1.79 * 10^{-3}$
5	6	0	$3.36 * 10^{-4}$
5	7	$4.27 * 10^{-4}$	$2.13 * 10^{-3}$
6	7	$4.27 * 10^{-4}$	$2.12 * 10^{-3}$
5	Ambient	$4.78 * 10^{-3}$	$4.39 * 10^{-3}$
6	Ambient	$4.78 * 10^{-3}$	$4.41 * 10^{-3}$
7	Ambient	$4.27 * 10^{-4}$	$4.26 * 10^{-3}$
8	5	$6.92 * 10^{-3}$	$6.53 * 10^{-3}$
8	6	$6.92 * 10^{-3}$	$6.53 * 10^{-3}$
9	10	$6.96 * 10^{-3}$	$9.02 * 10^{-3}$
11	9	0.75	0.75
11	10	0.75	0.75
9	Ambient	$7.43 * 10^{-1}$	$7.41 * 10^{-1}$
10	Ambient	$7.43 * 10^{-1}$	$7.41 * 10^{-1}$
10	12	$1.40 * 10^{-2}$	$1.82 * 10^{-2}$
(Ceiling) 12	8	$1.40 * 10^{-2}$	$1.82 * 10^{-2}$
(Ceiling) 8	4	$1.58 * 10^{-4}$	$5.1 * 10^{-3}$

Table 4.10: Mass flow rate (kg/s) Comparison between Network and CONTAM.

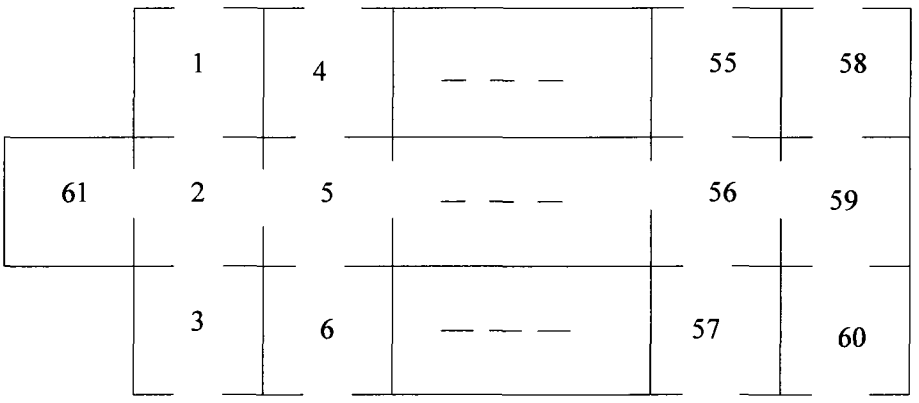

Figure 4.8: Geometry of 1-storey 61-room building

This building is designed to test multi-compartment buildings on network model. Both isothermal and non-isothermal cases are simulated here. Initial pressures and temperatures for all compartments are set to be ambient pressure and temperature.

– Isothermal case

In this case, compartment-61 gets a constant mass source of $1.5Kg/s$ with ambient temperature $293K$. Figure 4.9 shows a visualization of the simulation. Table 4.12 shows how the mass distributes from its source in compartment-61. Table 4.13 shows that there is no temperature changes during the simulation.

Simulation time (as reported from computer) of this case (for 1000 seconds) takes 24 min.

	Width(m)	Depth(m)	Ceiling Height(m)	Floor Elevation(m)
1	4	4	3	0
2	4	4	3	0
.	.	.	.	.
.	.	.	.	.
.	.	.	.	.
60	4	4	3	0
61	4	4	3	0

Table 4.11: Compartment dimension of the 61-room 1-storey Building.

From(room)	To(room)	Mass flow rate(kg/s) -Isothermal case	Mass flow rate(kg/s) -Non-isothermal case
61	2	1.5	1.5
2	1	0.45	0.46
2	3	0.45	0.46
1	Ambient	0.45	0.46
3	Ambient	0.45	0.46
2	5	0.59	0.59
5	8	0.23	0.23
8	11	0.09	0.1
11	14	0.04	0.05
14	17	0.01	0.02
17	20	0.006	0.006
56	59	0	0

Table 4.12: Mass flow rate for 1-storey 61-room building.

Compartment	Temperature (K) -Isothermal case	Temperature (K) -Non-isothermal case
61	293	350
1	293	348.5
2	293	350
3	293	348.5
5	293	349.4
8	293	331.7
11	293	304.6
14	293	294.4
17	293	293.1
20	293	293
56	293	293
59	293	293

Table 4.13: Temperature for 1-storey 61-room building.

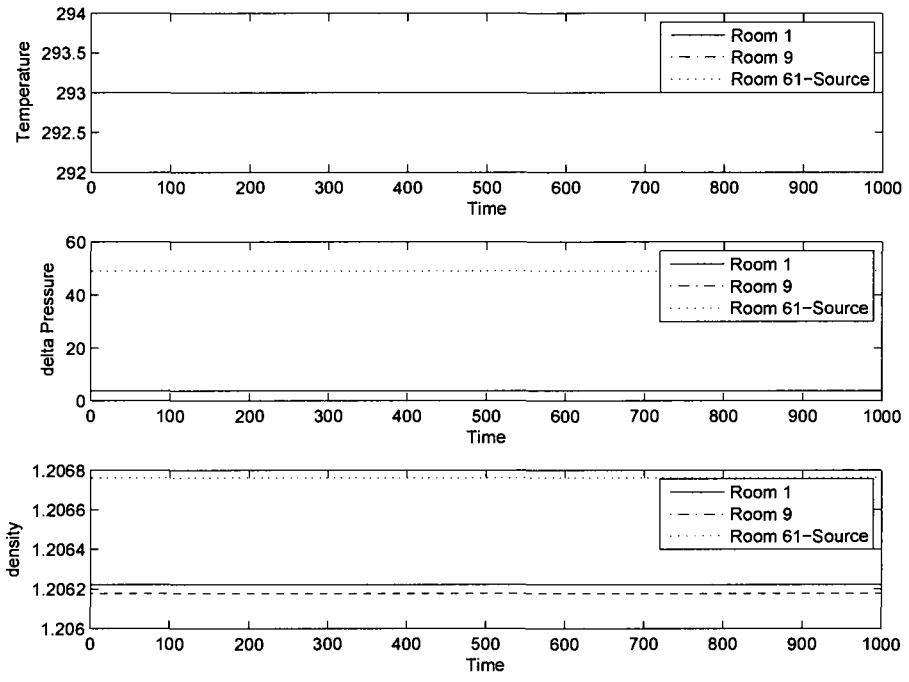

Figure 4.9: Plot for 1-storey 61-room building - isothermal case. (Temperature in K, Pressure in Pa, Density in Kg/m^3, Time in s)

– Non-isothermal case

In this case, compartment-61 gets a constant mass source of $1.5Kg/s$ with high temperature $350K$. Figure 4.10 shows visualization of the simulation, Mass distribution and temperature solution are shown in Table 4.12 and Table 4.13.

Simulation time (as reported form computer) for this case (of 1000 seconds) takes 132 min.

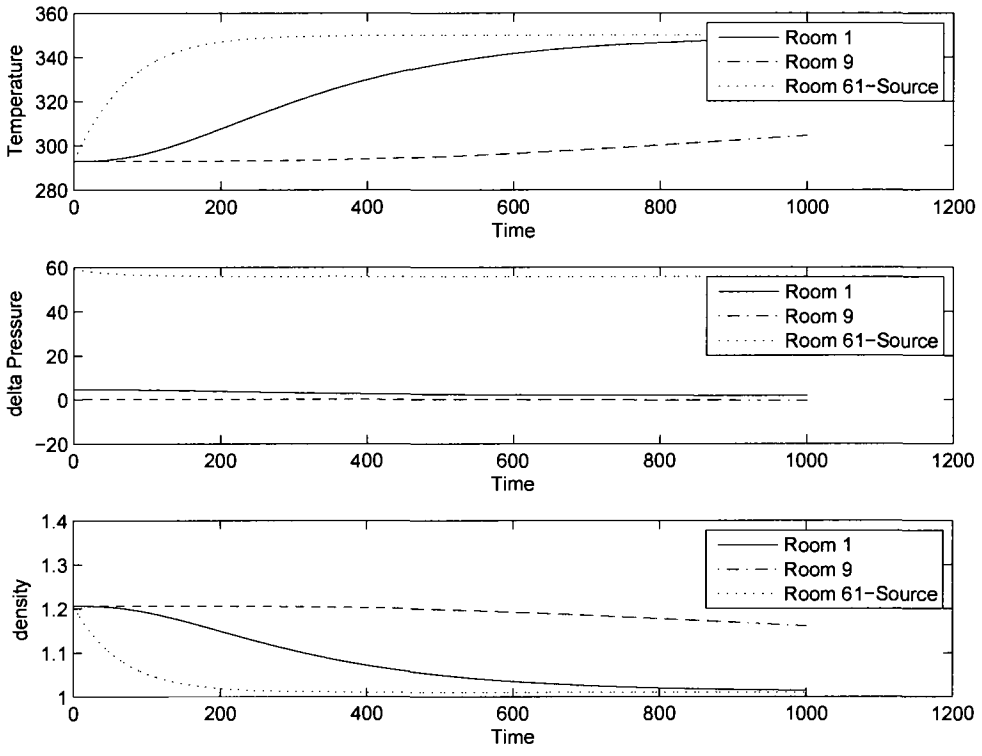

Figure 4.10: plot for 1-storey 61 rooms building - non-isothermal case. (Temperature in K, Pressure in Pa, Density in Kg/m^3, Time in s)

Ten-storey smoke tower

- Geometry of the building

  A ten-storey 52-room tower is designed here. Figure 4.11 to Figure 4.14 show the geometry of the building, Table 4.14 to Table 4.17 show the dimensions for compartments, corridors and stair shaft of this building.

	Width(m)	Depth(m)	Ceiling Height(m)
Compartment	3.78	9.643	3.3
Room 1	2.3	1.09	3.3
Stair shaft	5	2.68	3.3
Room 2	2.4	2.85	3.3
Corridor	24.1	1.17	3.3

Table 4.14: Compartment dimension of the 10-storey tower - 1st floor

	Width(m)	Depth(m)	Ceiling Height(m)
Compartment	3.78	8.9	3.3
Room	2.3	1.09	3.3
Stair shaft	5	2.46	3.3
Corridor 1	13.8	1.17	3.3
Corridor 2	13.8	1.17	3.3

Table 4.15: Compartment dimension of the 10-storey tower - 2nd floor

	Width(m)	Depth(m)	Ceiling Height(m)
Compartment	3.78	8.9	2.4
Room	2.3	1.09	2.4
Stair shaft	5	2.46	2.4
Corridor 1	13.8	1.17	2.4
Corridor 2	13.8	1.17	2.4

Table 4.16: Compartment dimension of the 10-storey tower - 3rd-8th floor

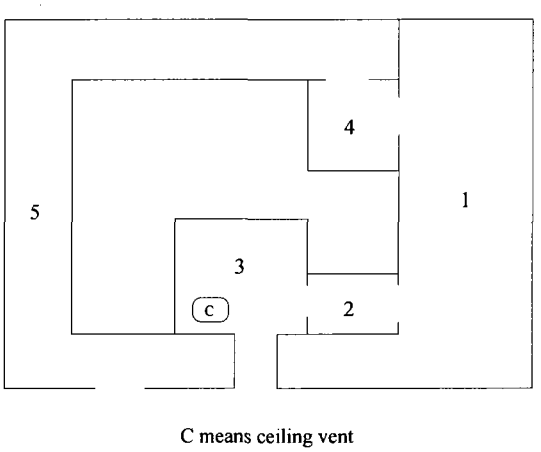

Figure 4.11: Floor plan of 10-storey tower - 1st floor

- Simulation

The purpose of this simulation is to test the 10-storey tower on network model. A constant mass source of $1.5Kg/s$ with high temperature $350K$ is placed into compartment-6 on the second floor of the tower. Initial temperatures and pressures for all rooms are ambient.

Figure 4.15 shows a visualization of the simulation, four compartments (each on different floor) are chosen and shown in the plot. Since compartment-6 gets the source, its temperature rises much faster compared to other rooms, while compartment-16 and compartment-21 being located far from the source, their temperatures rise very slowly. Table 4.19 shows temperature solutions for the main compartments on each floor. Note that temperature in compartment-1 barely changes during the simulation, this is because hot air only goes up (not down) through ceiling vents, therefore,

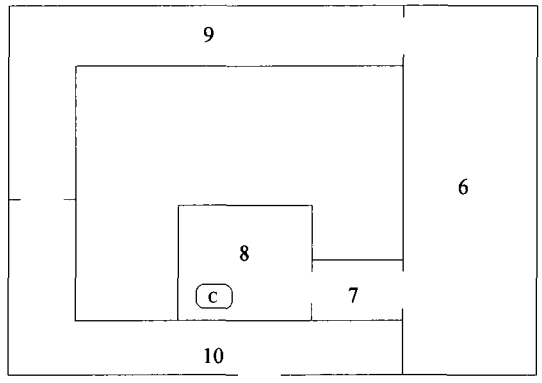

Figure 4.12: Typical 2nd - 8th floor plan of 10-storey tower - 2nd floor

compartment-1 which is underneath compartment-6 does not receive any hot air. Several windows/ceiling vents are chosen (shown in Table 4.18) to show the mass exchanges.

Simulation time (as reported from computer) for this case (of 1200 seconds) takes 15 min.

	Width(m)	Depth(m)	Ceiling Height(m)
Compartment	3.78	8.9	2.4
Room 1	2.3	1.09	2.4
Stair shaft	5	2.46	2.4
Corridor 1	13.8	1.17	2.4
Corridor 2	13.8	1.17	2.4
Room 2	2.4	2.85	2.4

Table 4.17: Compartment dimension of the 10-storey tower - 9th-10th floor.

Room ♯1	Room ♯2	Mass flow rate(kg/s) -from ♯1 to ♯2	Mass flow rate(kg/s) -from ♯2 to ♯1
6	7	0.47	0
7	8	0.47	0
6	9	1.03	0
12	13	0.35	0.51
16	17	0.33	0.39
47	48	0	0.04
51	53	0.04	0
(Ceiling)8	3	0.001	0
(Ceiling)8	13	0.47	0
(Ceiling)13	18	0.31	0
(Ceiling)18	23	0.25	0
(Ceiling)43	49	0.04	0

Table 4.18: Mass flow rate for 10-storey tower.

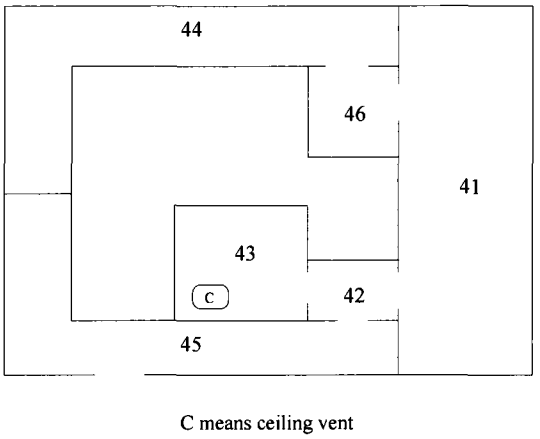

Figure 4.13: Floor plan of 10-storey tower - 9th floor

In this section, both the one-storey 61-room building and ten-storey tower cases show that our network model can be used for simulations on multi-storey buildings with a large number of compartments. However, the simulation time for these cases could be long due to their complexities. Next, we introduce adaptive time steps which could improve efficiency while maintain solution accuracy.

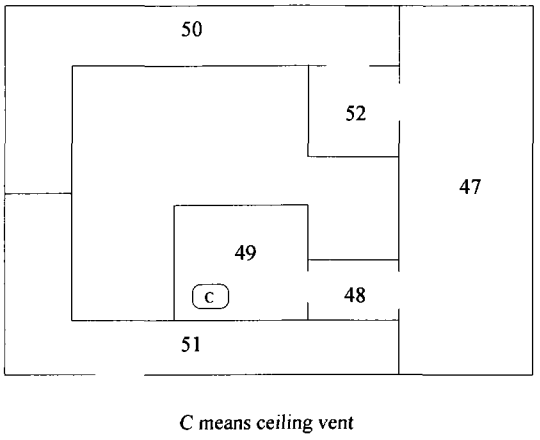

Figure 4.14: Floor plan of 10-storey tower - 10th floor

4.3 Comparison between Fixed Time Step and Adaptivity

Here is an example that demonstrates the improved efficiency of adaptive time steps over fixed time steps. Using the one-storey 61-room case, with the same initial time step (.001 seconds) and same simulation time (1000 seconds), a non-isothermal case is simulated here. Computer running times for fixed time step and adaptive time step are:

Running time for constant time step (as reported from computer) : 149min26s

Running time for adaptive time step (as reported from computer) : 13min7s

It is easily seen that adaptivity performs much faster than fixed time step.

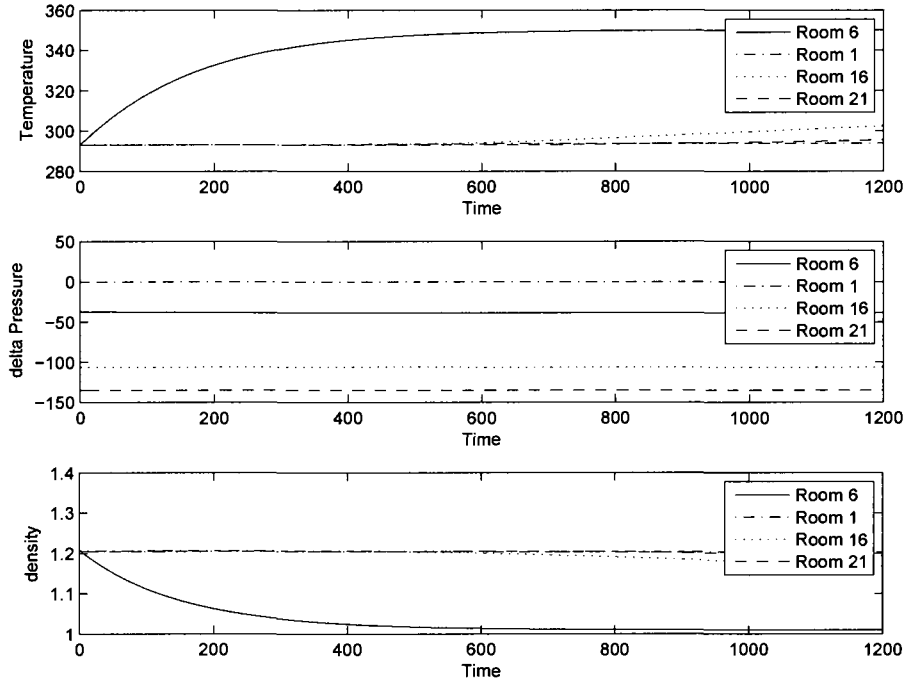

Figure 4.15: Plot for 10-storey tower - non-isothermal case. (Temperature in K, Pressure in Pa, Density in Kg/m^3, Time in s)

Compartment	Temperature (K)
1	293.8
6	350
11	309.1
16	302.4
21	295.5
26	293.6
31	293.1
36	293
41	293
47	293

Table 4.19: Temperature for 10-storey tower.

Moreover, the mass flow rate and temperature solution comparison shown in Table 4.20 and Table 4.21 imply that adaptive time steps maintain the same solution accuracy as fixed time steps. Figure 4.16 plots simulation time versus time step for adaptivity algorithms showing how time step changes along with simulation.

From(room)	To(room)	Mass flow rate-Adaptivity -Non-isothermal case	Mass flow rate-fixed time -Non-isothermal case
61	2	1.5	1.5
2	1	0.46	0.46
2	3	0.46	0.46
1	Ambient	0.46	0.46
3	Ambient	0.46	0.46
2	5	0.59	0.59
5	8	0.23	0.23
8	11	0.1	0.1
11	14	0.05	0.05
14	17	0.02	0.02
17	20	0.006	0.006
56	59	0	0

Table 4.20: Mass flow rate (kg/s) comparison (adaptivity vs fixed time step) for 1-storey 61-room building.

Compartment	Temperature (K)-Adaptivity -Non-isothermal case	Temperature (K)-fixed time -Non-isothermal case
61	350	350
1	348.5	348.5
2	350	350
3	348.5	348.5
5	349.3	349.4
8	331.9	331.7
11	304.9	304.6
14	294.4	294.4
17	293.1	293.1
20	293	293
56	293	293
59	293	293

Table 4.21: Temperature comparison (adaptivity vs fixed time step) for 1-storey 61-room building.

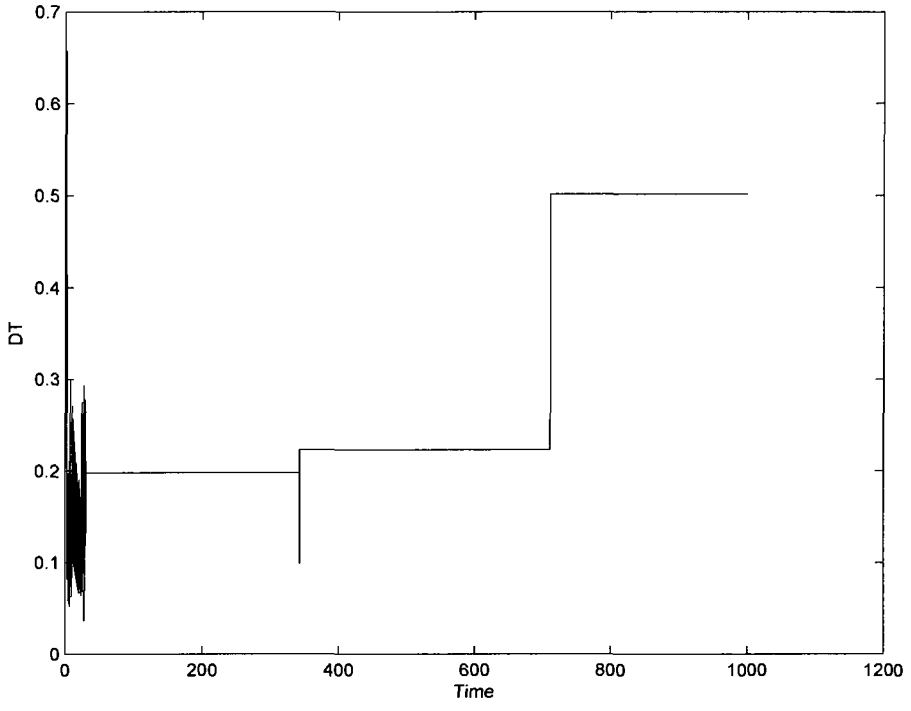

Figure 4.16: Time vs DT - 1-storey 61-room building

4.4 Integration of Two-Zone and Network Models

The final task is to combine two-zone and network models, so that users can simulate both models together.

The two-storey four-compartment building (for two-zone model) is used here for the two-zone model, and the ten-storey tower is used for the network model. Mass flow and upper temperature from compartment-3 (of two-zone model) are considered as sources, which are placed into compartment-6 of the ten-storey

Time(s)	Temperature (K)	Mass flow rate (kg/s)
0	293	0
50	417	1.02
100	423	0.56
150	421	0.29
200	442	0.36
250	450	0.38
300	452	0.37

Table 4.22: Mass source and temperature entering in Network model from 2-zone model.

tower. Temperature and mass source listed in Table 4.22 are generated by two-zone model, and become sources for the network model.

Figure 4.17 shows temperature and pressure changes of four compartments in ten-storey tower after receiving sources from the two-zone model. The results of mass flow rates and temperature solutions in Table 4.23 and Table 4.24 are reasonable, as rooms on higher floor get less mass flow and slower temperature increase.

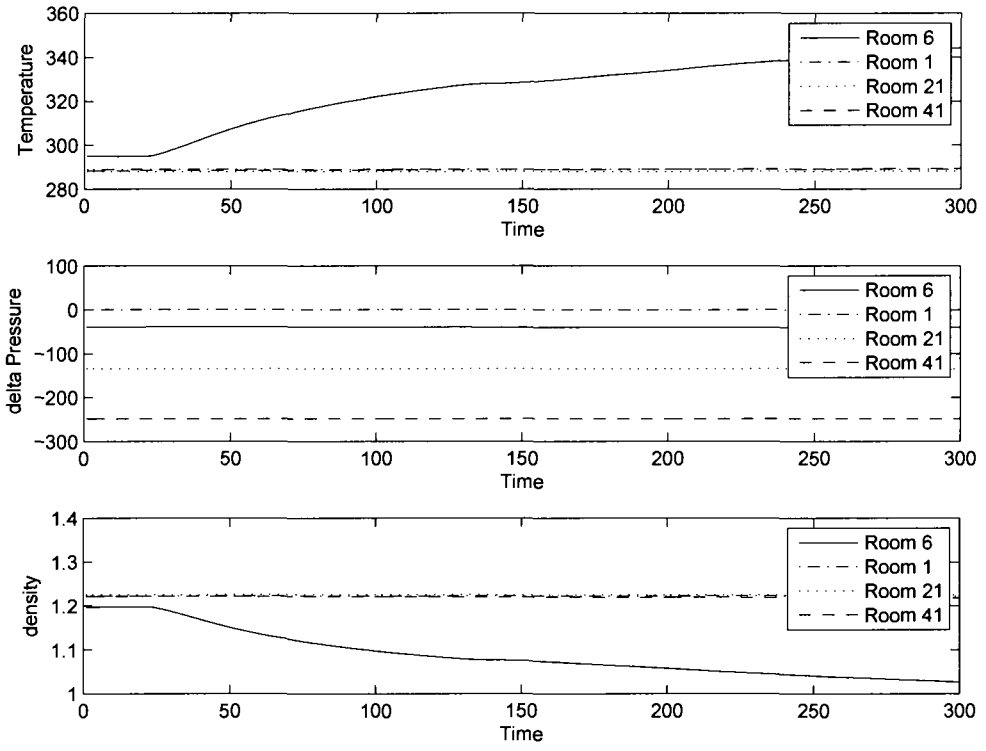

Figure 4.17: Plot for the hybrid model - 10-storey tower. (Temperature in K, Pressure in Pa, Density in Kg/m^3, Time in s)

Room ♯1	Room ♯2	Mass flow rate(kg/s) -from ♯1 to ♯2	Mass flow rate(kg/s) -from ♯2 to ♯1
6	7	0.66	0.06
7	8	0.82	0.22
6	9	0.18	0.37
12	13	0.1	0.64
16	17	0.07	0.37
47	48	0.11	0.003
51	53	0	0.1
(Ceiling)8	3	0	0.64
(Ceiling)13	8	0	1.25
(Ceiling)18	13	0	0.73
(Ceiling)23	18	0	0.44
(Ceiling)49	43	0.11	0

Table 4.23: Mass flow rate for 10-storey tower - hybrid model.

Compartment	Temperature (K)
1	289
6	344
11	290
16	289
21	288
26	295
31	289
36	289
41	289
47	291

Table 4.24: Temperature for 10-storey tower - hybrid model.

Chapter 5

Conclusion and Future Works

The objective of this research was to develop a hybrid model, combining a two-one and a network model, which simulate smoke and heat movement from fires in multi-compartment buildings.

5.1 Conclusion

Our two-zone model is developed to simulate the room with fire origin and compartments surrounding the fire room. The network model is developed to simulate compartments that are far away from the fire room. The main focus of the hybrid model is the development of the network model, unlike other network models that have limitations dealing with energy exchanges, our network model can predict both pressures and temperatures.

Various methods for solving linear and nonlinear equations have been reviewed, and we decided upon the choice of a Newton-GMRES method for solving pressure equations because of its fast convergence and its versatility to different building configurations. Temperature equations are then solved by a standard ODE solver, DLSODE.

We tested our model with simulations on different types of buildings, and comparisons with existing fire models are made in this thesis. The results show that our model provides good prediction of pressures and temperatures for multi-compartment buildings.

5.2 Future Works

Future work related to this research include

- Make code more robust to increasing building complexity.
- Make use of preconditioning in Newton-GMRES method to improve efficiency on solution convergence.
- Harmonize input file for two-zone and network models.
- Make code more user-friendly by requiring less user inputs.
- Refine parameters in adaptivity routine.

Bibliography

[1] Achakji, G.Y. & Tamura, G.T., (1994) *Pressure Drop Characteristics of Typical Stair Shafts in High-rise Buildings.* ASHRAE Transactions, 100-1223.

[2] Axelsson, O., (1994) *Iterative Solution Methods.* CAMBRRIDGE University Press.

[3] Babrauskas, V. (1979) *COMPF2- A Program for Calculating Post-Flashover Fire Temperatures.* NBS TN 991, National Bureau of Standards, Washington, DC.

[4] Babrauskas, V. & Williamson, R. B. (1978) *Post-Flashover Compartment Fires: Basis of a Theoretical Model.* Fire and Materials 2, 39-53.

[5] Barrett, R.E. & Locklin, D. W. (1969) *A Computer Technique for Predicting Smoke Movement in Tall Buildings, Symposium on Movement of Smoke on Escape Routes in Buildings.* Watford College of Technology, Watford, Herts, U. K., pp. 78-87

[6] Bilger, R.W. (1994) *Computational Field Model in Fire Research and Engineering. Proc. Fourth International Symp.* Fire Safety Science, June. pp 95-110.

[7] Butcher, E.G., et al. (1969) *Prediction of the Behavior of Smoke in a Building Using a Computer, Symposium on Movement of Smoke in Escape Routes in Buildings.* pp. 70-75, Watford, Herts, England: Watford College of Technology

[8] Cadorin, J-F. & Franssen, J-M. (2003) *A tool to design steel elements submitted to compartment fires-OZone V2. Part 1: pre- and post-flashover compartment fire model.* Fire Safety Journal 38 , 395-427

[9] Cetegen, B.M., Zukoski, E.E. & Kubota, T., (1984) *Entrainment in the near and far field of fire plumes.* Combustion Science & Technology, 39-305.

[10] Chow, W.K., (1996) *Multi-cell concept for simulating fire in big enclosures using a zone model.* J. Fire Sci. ;14(3):98-186.

[11] Cooper, L.Y., (1982) *Heat transfer from a buoyant plume to an unconfined ceiling.* ASME J. of Heat Transfer, 104-446.

[12] Cooper, L.Y., (1986) *The buoyant plume-driven adiabatic ceiling temperature revisited.* ASME J. of Heat Transfer, 108-822.

[13] Cooper, L.Y., (1989) *Calculation of the Flow Through a Horizontal Ceiling/Floor Vent.* National Institute of Standards and Technology, NISTIR 89-4052 .

[14] Cooper, L.Y., (1995) *Combined buoyancy and pressure-driven flow through a shallow, horizontal, circular vent.* Journal of Heat Transfer, 117-659.

[15] Cooper, L.Y., (1997) *VENTCF2: an algorithm and associated FORTRAN 77 subroutine for calculating flow through a horizontal ceiling/floor vent in a zone-type compartment fire model.* Fire Safety J., 28-253.

[16] Cooper, L.Y. & Forney, G. P.(1990) *Consolidated Compartment Fire Model (CCFM) Computer Code Application CCFM.VENTS. Part 1.* Physical Basis. NISTIR 4342; 96

[17] Cooper, L.Y., Harkleroad, M., Quintiere, J.G. & Rinkinen, W.J., (1982) *An experimental study of upper hot layer stratification in full-scale multi-room fire scenarios.* ASME Journal of Heat Transfer, 104-741.

[18] Cooper, L.Y. & Stroup, D.W. (1982) *Calculating Available Safe Egress Time (ASET)–A Computer Program and User's Guide.* NBSIR 82-2578; National Bureau of Standards, Washington, DC.137

[19] Cox, G. (1995) *Basic Considerations In Combustion Fundamentals of Fire.* Academic Press, London.

[20] Cox, G., Kumar, S. & Markatos, N.C. (1985) *Some Field Model Validation Studies, Proc. First International Symp.* Fire Safety Science, November, 159-171.

[21] Curtar, M.R. & Bodart, X.E. (1986) *1st Symposium International Association for Fire Safety Science.* Hemisphere Publications, Gaithersburg, MD, 637

[22] Davis, W.D. (1999) *The Zone Fire Model JET: A Model for the Prediction of Detector Activation and Gas Temperature in the Presence of a Smoke Layer.* NISTIR 6324; 55

[23] Dembsey, N.A. & Pagni, P.J. & Williamson, R.B.,(1995) *Compartment near-field entrainment measurements.* Fire Safety Journal, 24-383.

[24] Dietenberger, M.A., (1991) *Technical Reference and Users Guide for FAST/FFM Version 3.* NIST-GCR-91-589.

[25] Dols, W.S., Denton, K. R. & Walton, G. N. (2000) *CONTAMW User Manual.* National Institute of Standards and Technology, Gaithersburg, MD

[26] Evers, E. & Waterhouse, A. (1978) *A Computer Model for Analyzing Smoke Movement in Buildings.* Building Research Establishment., Borehamwood, Herts, U. K

[27] Feustel H.E. (1999) *COMIS - An International Multizone Air-flow and Contaminant Transport Model.* Energy and Buildings, v.30, pp.3-18.

[28] Floyd, J.E., Baum, H.R. & McGrattan, K.B. (2001) *A mixture fraction combustion model for fire simulation using CFD.* The International Conference on Engineered Fire Protection Design (San Francisco), June 11-15. 279-290

[29] Fu, Z. & Fan, W., (1996) *A zone-type model for a building fire and its sensitivity analysis.* Fire and Materials, 20-215.

[30] Fu, Z., Kashef, A., Benichou, N. & Hadjisophocleous, G.V.,(2002) *FIERAsystem Theory Documentation : Smoke Movement Model, IR-835.* National Research Council of Canada, Ottawa

[31] Jones,W.W., Peacock, R.D., Forney, G.P. & Reneke, P.A. (2005) *CFAST - Consolidated Model of Fire Growth and Smoke Transport (Version 6).* NIST Special Publication 1026, National Institute of Standards and Technology, Gaithersburg, MD

[32] Jones, W.W. (1985) *A Multicompartment Model for the Spread of Fire, Smoke and Toxic Gases.* Fire Safety Journal. Vol 9, 55-79

[33] Heskestad, G., (1995) *Fire plumes. The SFPE Handbook of Fire Protection Engineering.* Quincy, Mass.: National Fire Protection Association, 2-9.

[34] Holman, J.P., (1986) *Heat Transfer.* McGraw-Hill, 323

[35] Huggett, C., (1980) *Estimation of the rate of heat release by means of oxygen consumption.* J. of Fire and Flammability, 12.

[36] Kanury, A.M. (1987) *On the Craft of Modeling in Engineering and Science.* Fire Safety J., 12, 65-74.

[37] Karlsson, B. & Quintiere, J.G. & Enclosure Fire Dynamics, CRC Press 2002 Klote, J. H. (1982) *A Computer Program for Analysis of Smoke Control Systems.* National Bureau of Standards, NBSIR 82-2512.

[38] Kreith, F., (1976) *Principles of Heat Transfer.* 3rd edition. Intext Educational Publishers, New York.

[39] Liu, F. & Fu, X.Z. & Chow, W.K., (2001) *A Network Model of Simulation Smoke Movement in Buildings.* International J. on Performance-Based Fire Codes, vol 3, number 4, 151-157

[40] Liddament, M.W. (1996) *Guide to Energy Efficient Ventilation.* Air Infiltration Ventilation Centre.

[41] Lovatt, A., (1998) *Comparison studies of zone and CFD fire simulations.* Fire Engineering Research Report, University of Canterbury.

[42] Mathews, J.H. & Fink, K.D., (1999) *Numerical Methods Using MATLAB.* Prentice Hall.

[43] Mawhinney, N., Galea, E.R., Hoffmann, N. & Patel, M.K. (1994) *A Critical Comparison of a Phonetics Based Fire Field Model with Experimental Compartment Fire Data.* J. of Fire Protection Engineering, 6, 137-152.

[44] McCaffrey, B.J., (1983) *Momentum implications for buoyant diffusion flames.* Combustion and Flame, 52-149.

[45] Mitler, H.E. & Rockett, J. A. (1987) *Users' Guide to FIRST, A Comprehensive Single-Room Fire Model.* CIB W14/88/22 (USA); NBSIR 87-3595; 138

[46] Milter, H.E., (1985) *The Harvard Fire Model.* Fire Safety J., vol. 9, 7-16

[47] Motevalli, Y. & Ricciuti, C., (1992) *Characterization of the confined ceiling jet in the presence of an upper layer in transient and steady-state conditions.* NIST-GCR-92-613.

[48] Mowrer, F.W. & Williamson R.B., (1987) *Estimating room temperatures from fires along walls and in corners.* Fire Technology, 23-133.

[49] Parker, W.J., (1984) *Calculation of the heat release rate by oxygen consumption for various applications.* J. of Fire Sciences, 2-380.

[50] Peacock, R.D., Davis, S. & Babrauskas, V., (1991) *Data for room fire model comparisons.* J. of Research of the NIST, 96-411.

[51] Peacock, R.D., Forney, G.P., Reneke, P., Portier, R. & Jones, W.W., (1993) *CFAST, the Consolidated Model of the Fire Growth and Smoke Transport.* NIST Technical Note 1299.

[52] Pettersson, O., Magnusson, S.E. & Thor, J. (1976) *Fire Engineering Design of Steel Structures.* Publication 50, Swedish Institute of Steel Construction, Stockholm 1976.

[53] Quintiere, J.G., (1977) *Growth of Fires in Building Compartments. ASTM STP 614.* American Society for Testing and Materials, Philadelphia, PA.

[54] Saad, Y., (1996) *Iterative Methods for Sparse Linear Systems.* PWS Publishing Company.

[55] Sander, D.M. & Tamura, G. T. (1973) *FORTRAN IV Program to Stimulate Air Movement in Multi-storey Buildings.* National Research Council Canada, DBR Computer Program No. 35

[56] Siegel, R. & Howell, J., (1981) *Thermal Radiation Heat Transfer.* 2nd edition, Hemisphere Publishing Corporation.

[57] Stoer, J. & Bulirsch, R., (2002) *Introduction to Numerical Analysis* Springer.

[58] Tanaka, T. & Yamada, S., (2004) *BRI2002: Two Layer Zone Smoke Transport Model.* Fire Science and Technology, Vol.23, No.1 (Special Issue).

[59] Trefethen, L.Y. & Bau, D.III, (1997) *Numerical Linear Algebra.* SIAM

[60] Wade, C. (1999) *Branzfire-Engineering Software for Evaluating Hazard of Room Lining Materials.* J. of Fire Protection Engineering, 8(4), 183-193

[61] Walton, G.N. (1997) *CONTAM96 User Manual, NISTIR 6056.* National Institute of Standards and Technology, Gaithersburg, MD.

[62] Walton, G.N. (1989) *AIRNET - A Computer Program for Building Airflow Network Modeling.* National Institute of Standards and Technology.

[63] Wakamatsu, T. (1977) *Calculation Methods for Predicting Smoke Movement in Building Fires and Designing Smoke Control Systems.* Fire Standards and Safety, ASTM STP-614, A. F. Robertson, Ed., Philadelphia, PA, American Society for Testing and Materials, pp. 168-193

[64] Yao, J., Fan, W., Kohyu, S. & Daisuke, K.,(1999) *Verification and application of field-zone-network model in building fire.* Fire Safety J. vol-33; 35-44

[65] Yii, E.H., (2002) *Modeling the Effects of Fuel Types and Ventilation Openings on Post-Flashover Compartment Fires.* Fire Engineering Research Report, University of Canterbury, NZ.

[66] Zukoski, E.E., (1994) *Mass flux in fire plumes. Proceedings of the Fourth International Symposium on Fire Safety Science.* International Association for Fire Safety Science.